Drift mobility of amorphous semiconductors measured by the traveling-wave technique

Robert E. Johanson
The James Franck Institute, The University of Chicago, Chicago, Illinois 60637
(Received 15 July 1991; revised manuscript received 18 October 1991)

The traveling-wave technique for measuring drift mobility is examined within the context of practical application to thin films of low-mobility amorphous semiconductors. The basic theory that relates the drift mobility to the direct current produced by the nonlinear interaction of carriers with a traveling electric field is reviewed. Extending the theory to include carrier diffusion is shown to produce only small corrections even if the diffusion length exceeds the sample's thickness. The effect of an inhomogeneous conductivity on the direct current is computed and is shown to be small for an exponential conductivity profile, as would occur in an illuminated semiconductor. A general prescription is given for interpreting the traveling-wave drift-mobility measurements with an arbitrary model of charge transport. Two specific models are solved—multiple trapping and low-temperature hopping. Experimental techniques are then discussed in relation to sources of error. Examples are given of drift-mobility data for *n*-type *a*-Si:H from 200 to 450 K in the as-deposited state, after quenching, and after annealing at high temperatures. Finally, the data obtained from illuminated *a*-Si:H at temperatures down to 1.6 K are discussed.

I. INTRODUCTION

This paper investigates the drift mobility of charge carriers in low-conductivity amorphous semiconductors measured by the traveling-wave technique (TW). The drift mobility is defined as the average mobility of a group of charge carriers drifting in an electric field. The carriers may occupy various energy levels; hence the average mobility need not be that of any particular transport level such as the conduction or valence band. The particular energy levels populated by the carriers depend on the specific conditions of the experiment and, in particular, the manner in which the group of carriers is prepared. The traveling-wave technique utilizes the electric field associated with a surface acoustic wave (SAW) propagating on a piezoelectric plate to bunch carriers in a semiconductor into charge packets and drift these carriers through the material. A direct current is produced from which the drift mobility is calculated. This paper has three objectives. The first is a theoretical investigation of the acoustoelectric interaction emphasizing the practical consequences for extracting the drift mobility from measurements. To this end, a simple theory that ignores carrier diffusion is reexamined to provide a physical picture of where and how currents are generated in the semiconductor and the changes that occur as the conductivity of the semiconductor varies. The effects of carrier diffusion on the simple theory are then investigated. Further, numerical solutions are obtained for samples whose conductivity varies normal to the surface, as will be the case during illumination by strongly absorbing light or if band bending occurs at the surface. The second purpose is to demonstrate how particular models of charge transport are applied to the TW experiment in order to interpret the drift mobility. The multiple trapping model is solved for the TW case, and the drift mobility is found to be closely related to that measured by other techniques. A hopping model relevant to low-temperature photoconductivity is also solved. In this case, the drift mobility is dominated by carriers that hop at the frequency of the traveling wave. Finally, data obtained at low and high temperatures are presented along with the experimental techniques relevant to obtaining high-quality data. The data above 200 K are understood by the multiple trapping model. The data below 100 K show interesting and unexpected effects that are not fully understood.

SAW delay lines form the basis of many useful devices for ultrasonic signal processing[1] and as such, have been intensively studied. The geometry used for the present experiment where a semiconductor is placed near the surface of the delay line (Fig. 1) also has practical applications and has been the subject of theoretical and experimental investigations. Much of that work focuses on the attenuation or amplification of the SAW by a high-mobility semiconductor and the application of studying surface properties of the semiconductor.[2] Adler *et al.* applied this geometry to amorphous silicon (*a*-Si:H), a low-mobility semiconductor.[3] The interaction is simpler for this material since the attenuation of the SAW by the semiconductor is negligible, and only the effect of the traveling electric field on the semiconductor need be considered. However, much of the previous theoretical work is still relevant to this case, especially the solution for traveling charge waves in a semiconductor.[4]

The carrier drift mobility in thin films of amorphous semiconductors has been studied by the time-of-flight technique (TOF) as developed by Spear.[5] Since I will in certain places compare the traveling-wave experiment to TOF, a brief description of TOF is necessary. A sheet of carriers is created near one surface by a brief flash of strongly absorbed light. A voltage V applied across the thickness of the semiconductor causes the carriers to drift

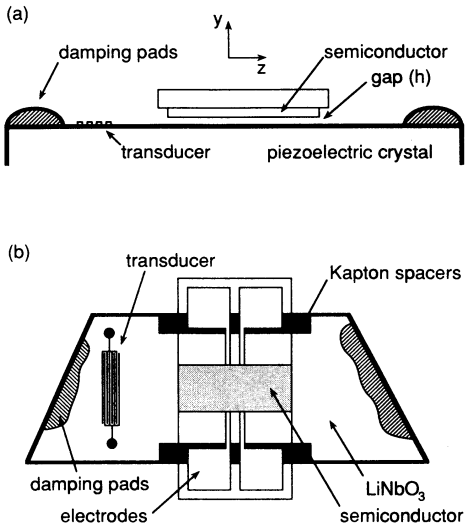

FIG. 1. A schematic diagram of the traveling-wave experiment, (a) side view, (b) top view. The $LiNbO_3$ is approximately 4 cm long and 2 cm wide.

to the other surface, and the average mobility of the carriers μ_d is obtained from the transit time t, $\mu_d = d^2/tV$, where d is the thickness. The progress of the carriers is monitored by the current induced in an external circuit as the charge sheet moves toward the electrode on the far surface. The drift mobility so measured is that of carriers in a highly nonequilibrium distribution that relaxes as the carriers traverse the sample. Proper interpretation of the drift mobility requires understanding the relaxation process. Much work has been done on the meaning of the drift mobility[6,7] and on the analyses of the current transients.[8,9] The principal information obtained is the nature and distribution of various energy states near the band edge since the carriers thermalize by interacting with these levels. In addition, the band mobility has been estimated.[10,11]

Although TOF has been successfully used to determine drift mobilities, limitations of the experiment demand that alternative techniques be developed. In particular, highly conducting samples with a dielectric relaxation time less than the transit time cannot be studied by TOF since the applied field collapses before the carriers are extracted. Also, samples composed of multiple layers of differing materials are unsuitable for TOF. TW overcomes these limitations and has been used to measure the drift mobility in doped a-Si:H at temperatures up to 450 K,[12–14] a-Si:H during illumination,[15] and a-Si:H/a-SiN_x multilayers.[16]

II. ELECTRIC POTENTIAL AND SPACE CHARGE WITHIN THE SEMICONDUCTOR

A. Surface charge theory

The relevant geometry of the traveling-wave experiment is shown in Fig. 1(a). A thin film of semiconductor, with thickness d and attached to a substrate, is placed a distance h above the surface of a piezoelectric plate. Transducers on the plate excite a surface acoustic Rayleigh wave that passes underneath the semiconductor. Due to the piezoelectric properties of the plate, there exists an electric field associated with the SAW that extends into the semiconductor. It is from the currents induced by this field that the drift mobility is calculated. In order to see why the drift mobility is related to these currents, the electric potential in the semiconductor must be determined given that the potential at the surface of the plate is

$$\phi_0 \exp[i(\omega t - kz)] \, . \tag{1}$$

The orientation of the axes is indicated in Fig. 1.

The current in a semiconductor with one kind of carrier and subject to an electric field $\mathbf{E}$ is

$$\mathbf{j} = -D\nabla\rho + \sigma\mathbf{E} + \mu\rho\mathbf{E} \, , \tag{2}$$

where D is the diffusion constant, σ is the conductivity due to the equilibrium carriers, ρ is the space charge density, and μ is the average mobility of the space charge. The sign of the last term is problematic. If the charge carriers are holes then a positive space charge represents an excess of carriers that contributes an additional current. However, for electrons, a positive ρ is a deficit of carriers that reduces the current; the sign of the term should be negative. Rather than change the sign of the term, let μ assume the sign of the carrier.

In the traveling-wave experiment, the space charge is induced by the electric field; therefore the last term in Eq. (2) is nonlinear in the field. An expression for ρ is derived below, and it is shown that the nonlinear term is usually small compared to the other two terms for the conditions encountered in the experiment. The nonlinear term is, therefore, dropped to simplify subsequent equations. The term should not be forgotten, however, as it is precisely this nonlinear interaction that results in the direct current that is measured in the experiment. The remaining expression for the current is inserted into the continuity equation;

$$\frac{\partial\rho}{\partial t} = -\nabla\cdot\mathbf{j} = D\nabla^2\rho - \sigma\nabla\cdot\mathbf{E} - \mathbf{E}\cdot\nabla\sigma \, . \tag{3}$$

For a homogeneous semiconductor, the conductivity has no gradient except, of course, at the surfaces; therefore the last term is zero within the semiconductor. The effects of an inhomogeneous conductivity are investigated below. Expressing the electric field and the space charge in terms of the potential yields the fundamental equation for the potential in the semiconductor;

$$\frac{\partial}{\partial t}\nabla^2\Phi_s = D\nabla^2\nabla^2\Phi_s - \frac{\sigma}{\epsilon\epsilon_0}\nabla^2\Phi_s \, . \tag{4}$$

An analytic solution is easily found; however, it is helpful to investigate the simple solution obtained in the limit $D \to 0$ where Eq. (4) reduces to the Laplace equation. It turns out that, for the purpose of evaluating the data, the error introduced by forcing D to zero is not significant. Fritzsche[17] has derived the solution for $D = 0$, so I will simply state the relevant results.

The solution of the Laplace equation that matches the boundary conditions must be a traveling wave;

$$\Phi_s = \{ A \cosh[k(y-h)] - B \sinh[k(y-h)] \} \times \phi_0 \exp[i(\omega t - kz)] \ . \quad (5)$$

Since the potential within the semiconductor is determined by the Laplace equation, there is no space charge. However, the last term of Eq. (3) cannot be ignored at the boundaries because the conductivity is obviously discontinuous. In order to balance the singularity in $\nabla\sigma$, ρ must also be singular; therefore, in the absence of diffusion, surface charge waves exist at each surface. The relations between the transverse electric field $E_y(y)$ and the surface charge per unit width at the surface nearer to (1) and further from (2) the piezoelectric plate are easily derived from charge continuity;

$$\delta_1 = -i(\sigma/\omega)E_y(h) = i(\sigma/\omega)kB\phi_0 \exp[i(\omega t - kz)] \ , \quad (6)$$

$$\delta_2 = i(\sigma/\omega)E_y(h+d) = i(\sigma/\omega)k(A \sinh kd - B \cosh kd)\phi_0 \exp[i(\omega t - kz)] \ . \quad (7)$$

The coefficients A and B are determined by the boundary conditions imposed on the electric field and by matching the solution of the Laplace equation in the gap to the potential at the surface of the piezoelectric plate. They are in general complex, indicating that the charge waves and the field have nontrivial phase relations. However, the complex part enters only through the complex dielectric constant;

$$\epsilon^* = \epsilon(1 - i\sigma/\epsilon\epsilon_0\omega) \ , \quad (8)$$

where ϵ is the real part of the semiconductor's dielectric constant.

Once the potential and the surface charge are determined from the linearized equations, we can return to the nonlinear term of Eq. (2) and ask what measurable currents are produced. The electric field oscillates at the frequency of the SAW as do all quantities that are derived from the linearized equations. The semiconductors studied have such high impedance that any alternating current cannot be measured. However, the ρE term of Eq. (2) is the product of oscillating quantities and produces a direct current providing the charge wave and the electric field do not differ in phase by $\pi/2$. The direct longitudinal current per unit width is obtained by averaging the product over a period;

$$I = \mu \langle \mathrm{Re}\delta \, \mathrm{Re}E_z \rangle_t \ . \quad (9)$$

Since there is a charge wave at each surface, there is also a direct current produced at each surface. Inserting the solutions into Eq. (9) yields

$$I_1 = \mu(\sigma k/v_s)(A \cdot B)\phi_0^2/2 \ , \quad (10)$$

$$I_2 = \mu(\sigma k/v_s)[(|A|^2 + |B|^2)\cosh(kd)\sinh(kd) - (A \cdot B)\cosh(2kd)]\phi_0^2/2 \ , \quad (11)$$

and the sum is the closed circuit current that is measured;

$$I_{\mathrm{AE}} = \mu(\sigma k/v_s)\sinh(kd)[(|A|^2 + |B|^2)\cosh(kd) - 2(A \cdot B)\sinh(kd)]\phi_0^2/2 \ , \quad (12)$$

where v_s is the velocity of the SAW. (The AE subscript is short for acoustoelectric). Because of the triangle inequality $|A|^2 + |B|^2 \geq 2A \cdot B$, the quantity in the brackets is strictly positive. The sign of I_{AE} is, therefore, the same as the sign of μ, defined to be the sign of the carrier, for a SAW traveling in the $+z$ direction. If the SAW travels in the $-z$ direction, the negative of Eq. (12) would have been obtained. But since the direction of the SAW is obviously under experimental control, a measurement of I_{AE} determines whether electrons or holes are the dominant equilibrium carrier.

For open circuit conditions, a voltage is produced;

$$V_{\mathrm{AE}} = (L/d)(I_{\mathrm{AE}}/\sigma) \ , \quad (13)$$

where L is the distance between electrodes. Notice that the σ that appears in Eq. (13) is the dc conductivity; whereas, in all the previous equations, σ is the ac conductivity at the frequency of the traveling wave. If the ac conductivity is not known and differs from the dc conductivity, the measured mobility will be in error by a factor $\sigma_{\mathrm{ac}}/\sigma_{\mathrm{dc}}$.

Equation (12) allows μ to be calculated from I_{AE} as all the other quantities are either known or measurable. Despite the approximations made in the derivation, the equation turns out to be quite accurate and is used in the following sections to convert the measurements to mobility. The further refinements of the theory—including the effects of carrier diffusion or an inhomogeneous conductivity—are compared to Eq. (12).

Typically, the traveling-wave experiment is used to investigate the temperature dependence of the mobility. Over the temperature range usually studied, the conductivity of a-Si:H—the material of concern—can vary by many orders of magnitude. The conductivity enters the equations in two places: the multiplying factor in the formulas for the surface charge density, Eqs. (6) and (7), and the imaginary part of the complex dielectric constant, Eq. (8). It is the latter that results in interesting effects once the conductivity exceeds a critical value that must be explored. Notice that the relative size of the imaginary part of ϵ^* is given by the ratio between the time scale for forming the regions of surface charge, namely ω^{-1}, and the dielectric relaxation time of the equilibrium carriers, $\epsilon\epsilon_0/\sigma$. If $\sigma \ll \epsilon\epsilon_0\omega$ then the dielectric constant is predominantly real, and the semiconductor, in its influence on the traveling electric field, acts like a simple dielectric insulator. The coefficients A and B are also predominantly real and independent of σ. The amplitudes of the surface charge waves simply scale with the conductivity; that is, they remain a constant fraction of the equilibrium carrier density, and the charge waves are in phase with E_z, which is optimal for producing a direct current. If $\sigma \gg \epsilon\epsilon_0\omega$ then ϵ^* is predominantly imaginary, and the material behaves more like a metal. A and

B have significant imaginary parts leading to changes in the phase relations between the charge waves and the field, which decrease I_1 and I_2. In addition, the charge on the near surface screens the field diminishing the charge and the current at the far surface. Once the field has been completely screened, the charge wave at the near surface does not continue to scale with conductivity but remains constant.

Figures 2–4 demonstrate these effects using realistic values for the variables. SAW frequencies are typically tens of megahertz. The value 18 MHz is used in the calculations, which is the frequency used to obtain most of the data analyzed in the following sections. The time scale is then fixed at $\omega^{-1}=9$ ns. Since $\epsilon=12$ for a-Si:H, the conductivity separating dielectric from metallic behavior is about 10^{-4} S cm^{-1}, a value that is exceeded by n-type a-Si:H within the experimental temperature range.

The ratio $(|\delta_1|-|\delta_2|)/|\delta_1|$ probes the screening of the field by the charge at the near surface because the charge density is directly related to E_y, Eqs. (6) and (7). A value of one indicates no charge—and, therefore, no field—at the far surface; the field is completely screened, whereas a value near zero denotes almost equal charge at both surfaces and little screening. For small σ, the far-surface charge is less than the near-surface charge by an amount that depends on the sample thickness because the field diminishes away from the piezoelectric plate with a decay length given by $k=(30\ \mu\text{m})^{-1}$. Above a certain σ that depends on thickness, the fraction of charge at the far surface decreases indicating screening (the dashed lines in Fig. 2). For a 1-μm-thick sample, significant screening occurs for $\sigma > 3\times10^{-3}$ S cm^{-1}.

The phase difference between the charge wave and E_z is also affected by sufficiently large σ (Fig. 3). The direct currents I_1 and I_2 are proportional to the cosine of the phase difference. The phase changes at both the near and far surfaces for $\sigma > 10^{-5}$ S cm^{-1} reducing both currents. However, the phase difference returns to zero for the near surface beginning at a σ that depends on thickness, 5×10^{-4} S cm^{-1} for a 1-μm-thick sample. The charge

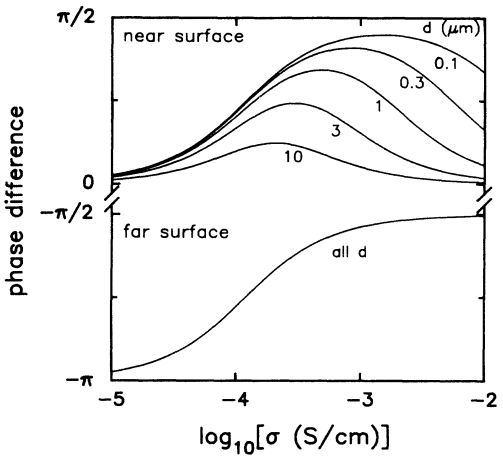

FIG. 3. The phase difference between the surface charge wave and E_z at the near and far surfaces as a function of conductivity for various semiconductor thicknesses d. The direct currents at each surface, I_1 and I_2, are proportional to the cosine of the phase difference.

and field remain out of phase at the far surface however large σ becomes. Also notice that the phase difference at the far surface is π for small σ and never becomes less than $\pi/2$. The current at the far surface has, therefore, the opposite sign of the current at the near surface; the total current is the sum of two opposing currents.

The net effect of the screening and the phase shifts is gauged by the fractional difference $(I_1+I_2)/I_1$ (the solid lines in Fig. 2). The current at the near surface is always larger in magnitude, so the ratio is positive; but, for small σ, the fractional difference depends on the sample thickness and amounts to only 8% for a 1-μm-thick sample. The near cancellation of I_1 and I_2 presents an acute difficulty should the mobilities of carriers at the near and far surfaces differ. Even a small imbalance would greatly affect the measured current, resulting in an erroneous

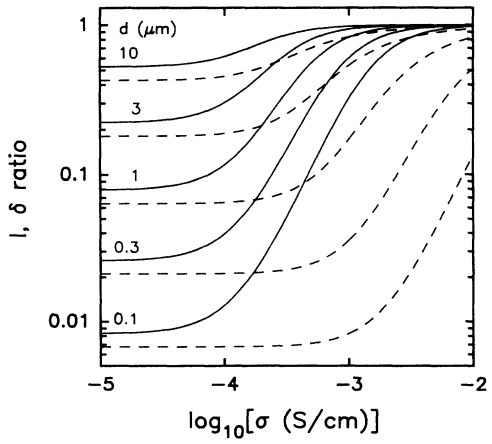

FIG. 2. The ratios $(I_1+I_2)/I_1$ (solid line) and $(|\delta_1|-|\delta_2|)/|\delta_1|$ (dotted line) as a function of conductivity for various semiconductor thicknesses d.

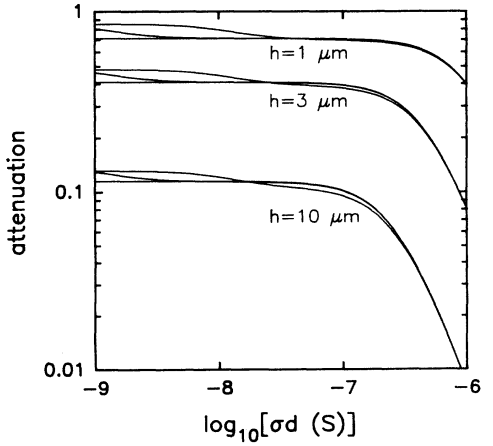

FIG. 4. The attentuation factor, the quantity in the brackets of Eq. (12), as a function of the sheet conductivity σd for several values of h as indicated. For each value of h, three curves are calculated for sample thicknesses of 0.01, 0.1, and 1 μm.

mobility value. For example, if, for some reason, the mobility at the far surface is suppressed by 4% for a 1-μm-thick sample, I_{AE} will change by 50%. For large σ—above 4×10^{-4} S cm^{-1} for a 1-μm-thick sample—the phase relations and the screening cause I_1 to become much larger in magnitude than I_2 as shown by the fractional difference approaching one in Fig. 2. The mobility at the far surface obviously becomes unimportant, and the measured mobility is accurately that of the near-surface carriers. This provides a unique opportunity to test sensitively if the mobilities are different at the two surfaces using a sample whose conductivity varies from the screening to the dielectric region as the temperature is lowered. Any difference results in an unusual jump in the measured mobility from that of the near surface to an erroneous value as the conductivity goes through the critical value.

The result of the screening and phase shifts on I_{AE} and V_{AE} is contained in the behavior of the quantity within the brackets in Eq. (12)—called the attenuation factor because it shows how much the signal is reduced by the effects of high conductivity. Remarkably, the attenuation factor is almost independent of thickness for $kd \ll 1$ if viewed as a function of σd (Fig. 4). At low temperatures where the conductivity is small, the attenuation factor is constant. I_{AE} is proportional to $\mu\sigma$ and increases rapidly with temperature since both the mobility and conductivity are usually activated. V_{AE} is proportional to μ. At higher temperatures, once $\sigma d > 10^{-7}$ S, the falling attenuation factor competes with the rising $\mu\sigma$ and, for doped a-Si:H, usually wins. It is not unusual for I_{AE} to slowly decrease with increasing temperature, whereas V_{AE} then falls rapidly. But, as long as both I_{AE} and V_{AE} can be accurately measured, the mobility can be calculated from the above formulas.

B. Diffusion

The solution given above omits the effects of charge diffusion with the result that the charge waves produced by the traveling electric field are confined to the surfaces. Diffusion has the effect of smearing the δ functions of charge into the interior of the semiconductor so that the charge occupies a certain width near each surface. Although a singularity in the charge density is obviously incorrect for a semiconductor, diffusion is expected to have a minimal effect on I_{AE} even if the charge waves at the near and far surfaces overlap. Diffusion redistributes the surface charge but essentially does not alter the amount, and since E_z changes only slowly with y, the value of I_{AE}, which is proportional to the charge times E_z, should be nearly independent of the diffusion constant. However, there are four reasons to proceed with the solution that includes diffusion. First, it is important for the analysis of data to confirm that diffusion does not affect the relation between I_{AE} and mobility to any significant extent since, in order to reduce the amount of computation, measurements are converted to mobility using the surface charge equations. Second, the surface of a semiconductor is often physically different from that of the bulk; in particular, surface states may act as additional trapping sites reducing the mobility near the surface. Knowing how the charge is actually distributed in the semiconductor allows one to gauge whether the measured mobility is characteristic of the bulk or the surface. Third, the nonlinear term in Eq. (2), ignored in solving for the potential, is proportional to the space charge density, and a value for ρ is needed to assess the importance of the nonlinearity. Finally, if the diffusion-induced space charge width is greater than the sample's thickness then the charge waves extending inward from each surface overlap and partially cancel one another. The effect on I_{AE} turns out to be small; however, the data obtained for thin samples are shown to be more reliable than the surface charge theory predicts.

The solution of Eq. (4) in z and t still has the form of a traveling wave;

$$\Phi_s = \varphi(y)\phi_0 \exp[i(\omega t - kz)] . \tag{14}$$

The problem reduces to determining the functional form in the y direction $\varphi(y)$. Inserting this solution into Eq. (4) results in a fourth-order equation for $\varphi(y)$;

$$\varphi'''' - (2k^2 + i\omega/D + \sigma/\epsilon\epsilon_0 D)\varphi'' + (k^2 + i\omega/D + \sigma/\epsilon\epsilon_0 D)k^2\varphi = 0 , \tag{15}$$

where the primes designate derivatives with respect to y. The solution of this equation is a simple enhancement of the solution without diffusion, Eq. (5).[4] (The coefficients are, of course, different.)

$$\varphi(y) = A\cosh[k(y-h)] - B\sinh[k(y-h)] + \alpha\cosh[q(y-h)] - \beta\sinh[q(y-h)] , \tag{16}$$

where

$$q = (k^2 + i\omega/D + \sigma/\epsilon\epsilon_0 D)^{1/2} . \tag{17}$$

The four coefficients are determined by the boundary conditions. In addition to the usual boundary conditions on the potential is the constraint that the current in the y direction vanish at both boundaries. A nonzero y current at a boundary leads to a δ function of charge, which is not allowed in the presence of diffusion. Solving for the coefficients is straightforward but tedious, and little insight is gained from the formulas. Rather, the effects of diffusion can be better determined by computing the relevant physical quantities for realistic situations.

The direct current is produced by the same interaction of the charge wave with the longitudinal field as in the surface charge theory except now the charge and the current density are distributed throughout the semiconductor. I_{AE} is determined by an integral over the thickness;

$$I_{AE} = \int_h^{h+d} \mu \langle \mathrm{Re}(\rho)\mathrm{Re}(E_z)\rangle_t dy . \tag{18}$$

Expressing ρ and E_z in terms of the potential results in elementary integrals. Comparing Eq. (18) to the homologous expression derived without diffusion, Eq. (12), reveals the effect of diffusion on I_{AE}. For a 1-μm-thick

sample and a traveling-wave frequency of 18 MHz, diffusion typically suppresses I_{AE} by a small amount. For example, the decrease amounts to 5% for $\sigma = 10^{-5}$ S cm^{-1} and $D = 0.03$ cm^2 s^{-1}, and correspondingly less for smaller D. Remarkably, diffusion has hardly any effect on I_{AE} when the conductivity is large enough to produce screening. In all cases where the sample is thicker than the width of the space charge, using the surface charge equations to reduce the data is acceptable.

Diffusion introduces a new length scale $1/q$ that determines the decay of the charge density away from the surface. The magnitude of q depends on the same competition between the experimental time scale and the dielectric relaxation time as in the surface charge case. For small σ, the ω/D term of Eq. (17) dominates, resulting in a charge density that oscillates in the y direction (due to the imaginary part of q) inside an exponentially decaying envelope with a decay length

$$l_D \approx (D/\omega)^{1/2} . \tag{19}$$

D is obtained from the mobility using Einstein's relation. For $\mu = 1$ cm^2 V^{-1} s^{-1} and at room temperature, l_D is about 1500 Å. Since surface states are typically localized within a few angstroms of the surface, most of the charge is well away from the influence of the surface, and the drift mobility should be characteristic of the bulk. Even at 200 K where the electron drift mobility may be as low as 10^{-2} cm^2 V^{-1} s^{-1}, $l_D = 125$ Å. For large σ, the $\sigma/\epsilon\epsilon_0 D$ term is dominant, and the decay length becomes

$$l_D \approx (D\epsilon\epsilon_0/\sigma)^{1/2} . \tag{20}$$

In this case, q is chiefly real, so the charge density decreases exponentially and without oscillation away from the boundaries. In this regime, l_D is never less than 100 Å for a-Si:H, and this value is reached only for $\sigma = 10^{-2}$ S cm^{-1}, which is at the upper end of the range that allows a measurable V_{AE}. In all cases, the charge is spread over a volume beyond the influence of surface states, and traveling-wave mobilities should be as much characteristic of the bulk material as those obtained from time of flight.

The peak charge density can be estimated by equating the surface charge density, Eq. (6), with the integral over y of the exponentially decaying space charge;

$$\rho_{max} \approx \sigma E_y/\omega l_D . \tag{21}$$

This assumes that diffusion only redistributes the charge present when $D = 0$. If the space charges of the near and far surfaces overlap and partially cancel then the peak charge density is lower than this estimate. The value of ρ_{max} can be used to gauge the importance of the nonlinear term $\mu\rho\mathbf{E}$ in Eq. (2). Although not definitive, if the nonlinear term is smaller than the linear term $\sigma\mathbf{E}$ everywhere within the semiconductor then the solution to the linearized equations is probably valid; the most stringent test obviously occurs where the charge density is maximum. I have evaluated both terms for the standard conditions and samples used in the experiment and find that the nonlinear term is always smaller. The worst case occurs when μ is large. For example, the nonlinear term is smaller by a factor of 3 when $\mu = 2$ cm^2 V^{-1} s^{-1} at $T = 450$ K, $\omega = 18$ MHz, and $E_y = 500$ V cm^{-1}, and correspondingly less important at lower temperatures as the mobility falls. However, care must be exercised if materials with a larger mobility are studied. ρ_{max} should then be reduced by decreasing the power in the SAW which lowers E_y.

If the sample is sufficiently thick, the space charge associated with each surface remains separated. Once $l_D > d/2$, the charge waves overlap, and since they differ in phase by π, cancellation occurs reducing the charge density. This is clearly beneficial in reducing ρ_{max}. But the effect on I_{AE}, and thus the validity of Eq. (12), is not clear. Figure 5 shows the effect of diffusion as a function of sample thickness in the low-conductivity regime. The current is suppressed once the diffusion length is comparable to the thickness but only by at most 20% no matter how thin the sample. The reason there is not a larger effect is actually quite simple. Although the current density in the semiconductor is reduced as the charge waves overlap, the current density associated with the near surface is reduced by nearly the same amount as that at the far surface. The net current, I_{AE} remains relatively unchanged. Although I_{AE} is similar with and without diffusion, there is a large difference in interpretation. The surface charge theory predicts that I_{AE} is proportional to the sample thickness, but the surface currents I_1 and I_2 are relatively insensitive to thickness; I_2 simply approaches $-I_1$ with decreasing d. As a result, I_1 and I_2 very nearly cancel for thin samples making the residual current extremely sensitive to any perturbation of either surface current. For example, consider a sample 0.01 μm thick. I_1 and I_2 differ in magnitude by less than one part in a thousand. An aberrant change in either current by 0.1% is enough to introduce a 100% error in I_{AE}. Since it would be impossible to exclude confounding effects of

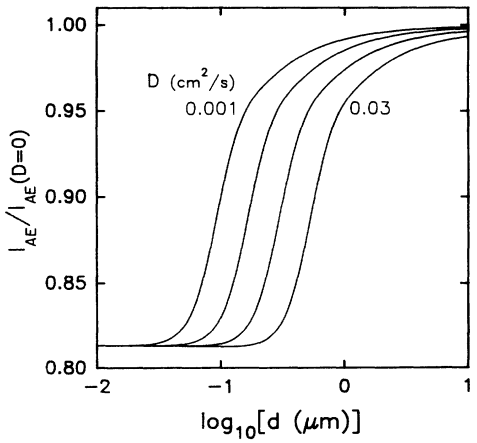

FIG. 5. The fractional change in I_{AE} due to diffusion as a function of sample thickness d for D equal to 0.001, 0.003, 0.01, and 0.03 cm^2 s^{-1}. The calculation uses a traveling-wave frequency of 18 MHz and a conductivity low enough to avoid screening. The limiting value of the ratio at small d occurs when the overlap of the space charge waves is such that only a single charge wave remains.

this magnitude, data for thin samples would be totally unreliable. Introducing diffusion, however, reverses this conclusion. For the same sample, once $D > 0.05\ \mathrm{cm^2\,s^{-1}}$, the charge from the near surface completely cancels the charge from the far surface leaving a single charge wave. The direct current density has the same sign throughout the sample, and I_{AE} is robust.

C. Inhomogeneous conductivity

The calculation of the current I_{AE} assumes that the conductivity is the same throughout the semiconductor, but this is not a good assumption in all circumstances. Surface states or a transfer of charge between the semiconductor and adsorbed material, oxide layers, or the substrate can lead to local fields and band bending. The region near the surface can be many orders of magnitude more or less conductive than the bulk of the film. Or when a sample is illuminated, the light intensity decreases exponentially through the material, and unless the absorption coefficient is small, the illuminated surface is more conductive than the back surface. A varying conductivity affects the traveling-wave experiment because the traveling electric field induces space charge wherever the gradient of the conductivity is nonzero. This space charge will contribute to I_{AE} in the same way as the charge at the surfaces; recall that the surface charge is a special case that exists because the gradient of the conductivity is singular at the surfaces. Since the conductivity profile is often not known, it is important to determine whether the relation between drift mobility and I_{AE} derived for the case of a homogeneous semiconductor, Eq. (12), remains approximately valid in the presence of conductivity gradients normal to the surface.

Rewriting the charge density and the electric field of Eq. (3) in terms of the potential in the semiconductor, Φ_s, and setting $D=0$ yields

$$-\epsilon\epsilon_0\frac{\partial}{\partial t}\nabla^2\Phi_s=\sigma\nabla^2\Phi_s+\nabla\Phi_s\cdot\nabla\sigma\ . \tag{22}$$

The last term on the right-hand side is important only if $\nabla\sigma$ is comparable to or larger than $k\sigma$. A thin film is unlikely to have such a large conductivity gradient parallel to the surface—in the x or z directions—so I assume σ varies significantly only in the y direction. The solution is a traveling wave with the form

$$\Phi_s=\varphi(y)\phi_0\exp[i(\omega t-kz)]\ . \tag{23}$$

Inserting this solution into Eq. (22) yields the differential equation for $\varphi(y)$:

$$\varphi''-k^2\varphi+\frac{\sigma'}{\sigma+i\omega\epsilon\epsilon_0}\varphi'=0\ , \tag{24}$$

where the primes designate derivatives with respect to y. Unfortunately, for most $\sigma(y)$ no analytical solution exists. However, numerical solutions for conductivity profiles of interest should be adequate to check whether Eq. (12) remains valid.

The potential is determined by numerically integrating Eq. (24) subject to the appropriate boundary conditions, and then I_{AE} is calculated from φ. If the conductivity is finite at the boundaries, there will still be surface currents per unit width (since diffusion is neglected). Inserting expressions for the surface charge density δ and E_z in terms of Φ_s into Eq. (9) results in the current at each surface in terms of φ;

$$I_{AE}^{\text{surface}}=\mp\frac{\mu\sigma}{v_s}\frac{\phi_0^2}{2}(\varphi\cdot\varphi')\ , \tag{25}$$

where the minus (plus) sign is for the near (far) surface. σ, φ, and φ' are evaluated at the particular surface. This expression is, of course, equivalent to Eqs. (10) and (11) of the surface charge theory where an analytic solution for φ exists. In addition to the surface currents, a new contribution to I_{AE} occurs wherever space charge exists as discussed above for the case of diffusion-induced space charge. Replacing ρ and E_z in Eq. (18) with the appropriate expressions in terms of Φ_s yields after some manipulation

$$I_{AE}^{\text{bulk}}=\mu\epsilon\epsilon_0 k\frac{\varphi_0^2}{2}\int_h^{h+d}\left[\frac{\sigma'}{\sigma+i\omega\epsilon\epsilon_0}\varphi'\right]\cdot(i\varphi)dy\ . \tag{26}$$

The total current is, of course, the sum of the two surface currents and the bulk current.

A fourth-order Runge-Kutta algorithm is used to integrate the differential equation (24) for the particular $\sigma(y)$ of interest with appropriate care to limit round-off error. The resulting φ is used to integrate Eq. (26) for the bulk current and is used in Eq. (25) for the surface currents. The total current thus obtained is what would be actually measured by the experiment. But, because $\sigma(y)$ is usually not known, Eq. (12) would be used to calculate a mobility from the current using the *average* value of the conductivity. If the mobility calculated in this way differs substantially from the true mobility then Eq. (12) cannot be used to analyze data for samples with a conductivity gradient greatly restricting the utility of traveling-wave measurements. The calculations below assume a sample 1 μm thick, a gap of 10 μm, and a traveling-wave frequency of 18 MHz.

I investigated several functional forms for the conductivity. A parabolic profile that reaches $\sigma_{\max}$ at the center and decreases to zero at the boundaries was used to test the numerical integration procedure. Since the conductivity is zero at the boundaries, only bulk direct currents are produced. However, the shape of the parabola approximates two surfaces resulting in two regions of current density of opposite sign analogous to the surface currents of a homogeneous sample. Numerical results confirm that Eq. (12) calculates a mobility within a few percent of the true mobility over a wide range of $\sigma_{\max}$ extending well into the high-conductivity region. The effect of the conductivity gradient is only to introduce a soft boundary which produces space charge waves with essentially the same net charge as those produced at the physical boundaries of a uniform sample.

More practical is a conductivity that decreases exponentially away from either the near or far surface with a decay constant q. Having the near surface more con-

ductive approximates the situation where certain gases are adsorbed on the free surface and charge is transferred to the semiconductor creating a conductive layer. A conductivity that decreases exponentially away from the far surface is obtained during illumination through the substrate—required by the geometry of the experiment—with the decay constant determined by the light's absorption coefficient. The exponential profiles can result in more severe gradients than a parabolic profile, and the large gradients are even better mimics of a boundary. Numerical calculations show that if $1/q > d$ or if the peak conductivity is small in the sense of not causing screening or phase shifts then Eq. (12) is accurate to within a few percent. The error increases to 20% for very narrow, very conductive channels, but this error is acceptable for most work considering that the drift mobility usually varies by several orders of magnitude over the temperature range studied. The error is due to the average conductivity being smaller than the conductivity of the narrow channel, which results in a miscalculation of the amount of screening and phase shifts. I conclude, though, that the presence of conductivity gradients does not invalidate the drift-mobility values calculated using the formula derived for the homogeneous case.

The above discussion assumes that despite the conductivity gradient the drift mobility of the carriers is the same throughout the semiconductor. This is reasonable in most cases since μ is controlled by the distribution of localized tail states and the band mobility, neither of which should be affected by band bending or illumination. The assumption is obviously false when extreme band bending produces an inversion layer since electrons and holes have different mobilities and also produce I_{AE} of opposite sign. However, I argue that even in this case Eq. (12) has validity. The reason is that an n-type layer must be separated from a p-type layer by an intrinsic layer with much lower conductivity. The conductivity gradients on either side of the intrinsic layer act as a boundary separating the inverted region from the bulk. As a result, each region produces its own current proportional to the mobility of the dominant carrier and with the sign of that carrier. The total current, however, will be dominated by the current from the layer with the larger conductivity and the measured mobility will be for carriers in this layer. Only in the unlikely event that the inverted region and the bulk have roughly the same conductivity-mobility product and thus produce equal and opposite currents will the measured mobility not represent the mobility of actual charge carriers.

III. INTERPRETATION OF THE DRIFT MOBILITY

The preceding section demonstrates that a mobility can be obtained from a measurement of I_{AE}, but it may not be clear exactly what the mobility is or how it relates to the drift mobility measured by TOF. As we shall see, the interpretation of the mobility depends on the particular type of charge transport taking place; however, a number of general observations can be made at this stage. First, μ enters in Eq. (2) as the mobility of carriers making up the space charge. The equilibrium carriers do not contribute to the direct current. Therefore the solution of any transport model must focus on the deviations from equilibrium induced by the traveling wave. Second, the charge waves are formed from the transverse currents, Eqs. (6) and (7), and not simply translated along the sample from electrode to electrode. The drift velocity of the carriers is typically several orders of magnitude less than the SAW velocity. This means that the regions of negative and positive charge are being continually recreated by injection and extraction of equilibrium carriers once each cycle. By this process, a natural time scale, ω^{-1}, is introduced in what may seem a steady-state measurement. Third, the injected carriers enter the space charge regions at the transport level—for example, the conduction band—and often start out in a distribution far from equilibrium that relaxes over the cycle. This is similar to the TOF experiment where the nonequilibrium distribution is created by the initial flash of light and the relaxation is monitored by the transient current as the carriers move through the sample. Finally, the mobility is an average over all the carriers making up the charge wave.

The general approach is as follows. The transport levels through which the carriers are injected into the charge wave need to be identified; usually these are the same as the levels responsible for the ordinary conductivity. This determines the initial carrier distribution. The carriers then relax by interacting with other levels, and the rate equations for these levels are solved for the occupation function. The injection and extraction of carriers by the traveling wave is introduced into the rate equations for the transport levels by an additional oscillating term. The oscillating part of the resulting occupation function is the deviation from equilibrium caused by the charge wave, showing exactly how the carriers in the charge wave are distributed over the various levels at any point in the cycle. The drift mobility is then obtained by averaging the mobility of every excess carrier with due consideration for the phase relation to E_z.

A. Mobility at high temperatures—multiple trapping transport

Transport via the extended states dominates at sufficiently high temperatures, and hopping among localized states does not significantly contribute to transport. Carriers can, however, be trapped into the localized states for a period of time, eventually being thermally reexcited to the transport level. The average mobility of the carrier is thereby reduced from the band mobility by the fraction of time spent immobile in the localized states. Such multiple trapping transport has been extensively studied especially in application to the TOF experiment.[6,7] In order to understand the traveling-wave mobility at high temperatures, the multiple trapping equations need to be solved considering the periodic injection of carriers by the traveling wave.

Since there is no hopping among localized states, the rate equation for the electron density of a particular energy level in the gap $n(\varepsilon)$ depends only on emission to and capture from the conduction band. (The equations are written assuming electrons are the dominant carrier. The

case for holes is similar.) Written in terms of the occupation function $f(\varepsilon)$ and density of states $g(\varepsilon)$, the rate equation is

$$\frac{dn(\varepsilon)}{dt}=\{b_n n_c g(\varepsilon)[1-f(\varepsilon)]\} - \{g(\varepsilon)f(\varepsilon)\nu_n \exp[(\varepsilon_c-\varepsilon)/k_BT]\} \quad (27)$$

where the first term in braces represents capture and the second, emission. The rate free electrons are captured is the product of the density of free electrons, n_c, the density of empty traps at this energy, and a constant proportional to an effective cross section for capture b_n. I assume the same cross section for every localized state. The thermal emission rate equals the product of the density of trapped carriers, an attempt to escape frequency ν_n, and a Boltzmann term. Equation (27) represents an infinity of rate equations, one for each energy level in the gap. However, the only coupling between the different levels is through the free electron density, which allows each level to be solved separately.

In the absence of the traveling electric field, the occupation function and the free electron density are constants in time. The traveling wave induces oscillating parts to these quantities which represent the changes due to the extra carriers in the space charge. Since the constant part of n_c does not contribute to I_{AE}, it is advantageous to separate the time-dependent parts, denoted by δ, from the constant or equilibrium solution, denoted by zero subscripts;

$$f(\varepsilon)=f_0(\varepsilon)+\delta f(\varepsilon) , \quad (28)$$

$$n_c=n_{c_0}+\delta n_c . \quad (29)$$

The equilibrium occupation function would normally be the Fermi function but would have a different form if, for example, the semiconductor is illuminated. I shall consider an unilluminated semiconductor in which case the equilibrium free electron density is

$$n_{c_0}=N_c \exp[(\varepsilon_c-\varepsilon_F)/k_BT] , \quad (30)$$

where N_c is the effective number of states in the conduction band which is usually taken to be k_BTg_c; g_c is the density of states at the mobility edge. Also detailed balance requires

$$b_n=\nu_n/N_c . \quad (31)$$

Rewriting the rate equation in terms of the varying quantities yields

$$\frac{d\delta f}{dt}=b_n\delta n_c(1-f_0)-b_n n_{c_0}\delta f - \delta f \nu_n \exp[(\varepsilon_c-\varepsilon)/k_BT]-b_n\delta n_c\delta f . \quad (32)$$

This would be a simple equation if not for the last term which is nonlinear since it depends on the product of oscillating quantities. However, the deviations from equilibrium are proportional to the strength of the traveling electric field which is controllable and can be made arbitrarily small. The nonlinear term, being the product of two small quantities, can always be made smaller than the other terms by a sufficiently weak electric field. I will assume that the experimental conditions are such that the nonlinear term has little influence and neglect it. Since the remaining equation is linear and since the space charge induced by the traveling electric field, which is what is driving the deviations from equilibrium, is sinusoidal in time, the solutions must also be oscillating with the same frequency. In order to simplify the equations, I redefine the variables as the magnitude and phase of the oscillations by extracting the time dependence;

$$\delta f \rightarrow \delta f \exp(i\omega t) \text{ and } \delta n_c \rightarrow \delta n_c \exp(i\omega t) . \quad (33)$$

Inserting these in the rate equation (32) and simplifying yields the relation between δf and δn_c for each energy level, that is, the normalized occupation function for the space charge in localized states $A(\varepsilon)$,

$$N_c\frac{\delta f}{\delta n_c}=\frac{1-f_0}{i\omega/\nu_n+\exp[-(\varepsilon_c-\varepsilon_F)/k_BT]+\exp[-(\varepsilon_c-\varepsilon)/k_BT]}=A(\varepsilon) . \quad (34)$$

The relative distribution of the space charge over the localized states is now known, and all that remains is to determine δn_c. I could solve the rate equation for the conduction band which includes not only the gain and loss of carriers from all the localized states but also the injection and extraction due to the traveling wave. However, this is unnecessary since the relative amount of charge in all other levels and the total charge is known. δn_c can be obtained by equating the total space charge $\rho\exp(i\omega t)$ with the sum of the excess free charge and the excess charge in the localized states;

$$\rho=-e\delta n_c-e\int^{\varepsilon_c} g(\varepsilon)\delta f(\varepsilon)d\varepsilon . \quad (35)$$

Inserting the solution for δf, Eq. (34), into Eq. (35) and solving for δn_c yields

$$\frac{-e\delta n_c}{\rho}=\left[1+\int^{\varepsilon_c}\frac{g(\varepsilon)}{N_c}A(\varepsilon)d\varepsilon\right]^{-1} . \quad (36)$$

Recall that the drift mobility is defined as the average mobility of all the carriers in the charge packet. The electrons that are in the conduction band move with the band mobility μ_0 while those in localized states are immobile. Therefore the drift mobility is simply μ_0 times the number of free electrons divided by the total number in the space charge packet. However, there is a subtlety that has been ignored. The preceding section explored

the phase relation between the charge wave and E_z, but it is possible that the mobile fraction of the charge wave is out of phase with the charge wave as a whole, that is, Eq. (36) may have an imaginary part. Only the part of δn_c in phase with E_z produces a direct current. In the low-conductivity region, the phase of E_z is zero. Thus the real part of δn_c is in phase with E_z. The drift mobility is then

$$\mu_d = \mu_0 \mathrm{Re} \frac{-e\delta n_c}{\rho} . \tag{37}$$

The main uses for drift-mobility measurements have been to determine the density of states (DOS) of the band tail and to measure μ_0. The ability of drift-mobility data to determine the DOS depends on the range of energy that contributes most to the integral in Eq. (36) and that in turn depends on the DOS, the shape of $A(\varepsilon)$, and how $A(\varepsilon)$ varies with temperature. If, for example, $A(\varepsilon)$ were a δ function at a certain energy then the mobility would be completely controlled by the DOS at that energy and no information could be obtained about the DOS elsewhere. Alternatively, if $A(\varepsilon)$ were flat then only the average DOS could be measured. Actually, $A(\varepsilon)$ lies between these two extremes as shown in Fig. 6. Above a demarcation energy given by

$$\varepsilon_d = \varepsilon_c - k_B T \ln(\nu_n/\omega) , \tag{38}$$

the excess carriers are in thermal equilibrium with the conduction band and, thus, have a Boltzmann distribution. Below the dark Fermi level, the occupation again drops off exponentially simply due to the lack of empty states. If the Fermi level is below ε_d then there is a region of states that can trap carriers but cannot establish thermal contact with the conduction band within one cycle of the wave. As a result, the occupation of these states by the excess carriers is out of phase with that above ε_d. Unfortunately, the band tail of a-Si:H is thought to rapidly decrease away from the band edge so

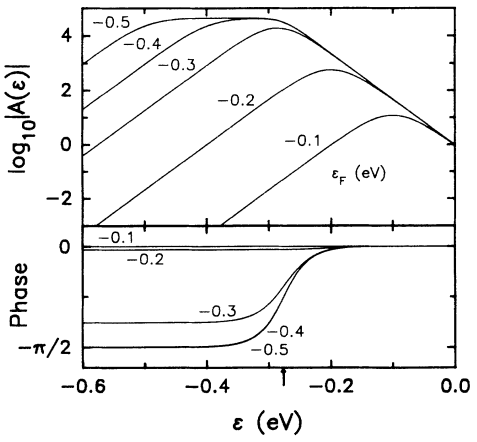

FIG. 6. Examples of the magnitude and phase of $A(\varepsilon)$, Eq. (34), calculated for various ε_F as indicated and using the following parameters: $T=300$ K, $\nu_n = 5\times10^{12}$ s^{-1}, and a SAW frequency of 18 MHz. The demarcation level, Eq. (38), is indicated by the arrow, ε is measured from the band edge ε_c.

that the integrand in Eq. (36) is the product of two functions that vary rapidly but in opposite directions. The result is that the place where the integrand peaks, and therefore, where information can be obtained about the DOS, depends on the details of the DOS itself and great care must be exercised when extracting DOS information from data.

B. Mobility at low temperatures—hopping transport

I now turn to a completely different type of transport that occurs in illuminated amorphous semiconductors at low temperatures. The photoconductivity of a-Si:H and many other amorphous semiconductors is strongly dependent on temperature except at the lowest temperatures where it becomes nearly constant.[18,19] The abrupt change in behavior suggests that the nature of the transport changes at low temperatures. It was originally postulated that charge transport at low temperatures occurs while the hot photoexcited electrons thermalize to the conduction-band edge after which they are rapidly trapped in localized, nonconducting states.[18] Although conduction during thermalization undoubtedly occurs, a recent theory considers hopping among the conduction band-tail states as the dominant mechanism which is the type of transport I consider here.[20]

In order to interpret the traveling-wave data obtained at low temperatures, a model of hopping transport is solved for the conditions of the experiment. I choose to investigate hopping for a number of reasons. At a few degrees Kelvin, the probability that an electron trapped in a band-tail state will be thermally reexcited to the mobility edge is negligibly small; therefore it is clear that a multiple trapping theory is inappropriate. The thermalization of hot electrons through the conduction band to the mobility edge is thought to be very fast, on the order of 1 ps, much faster than the natural time scale of the traveling-wave experiment which is the inverse of the traveling-wave frequency, $\omega^{-1}\approx 9$ ns. As will be shown below, the contribution to I_{AE} of an electron that spends such a short amount of time in a mobile level is strongly suppressed. Also, I find experimentally that I_{AE} does not depend on photon energy and thus on how high in the conduction band the electrons are excited which argues against a contribution during thermalization.

It is instructive to investigate first a simple example, namely, that of a single transport level, before dealing with a continuous distribution of localized states. Consider a single energy level into which electrons are generated at a rate G. The electrons can move while in the level with a mobility μ; it does not matter whether the transport occurs because the wave functions are extended or the electrons hop among localized states that make up the energy level. The electrons recombine or hop to a lower energy level after an average time τ. After leaving the transport level, the electrons remain immobile for the remaining cycle of the traveling wave. In the region near the surface, which contains the space charge packets, electrons are also alternately injected and extracted via the transport level by the traveling wave. All these processes lead to the rate equation governing the electron

density of the transport level;

$$\frac{dn}{dt}=-\frac{n}{\tau}+G+\frac{1}{e}\nabla\cdot\mathbf{j}\ . \tag{39}$$

The y component of the traveling electric field produces a current that has a divergence over a width Δ near the sample's boundaries producing the space charge;

$$\nabla\cdot\mathbf{j}=\frac{-\sigma E_y^0}{\Delta}\exp(i\omega t)\ . \tag{40}$$

The zero superscript refers to the amplitude of the field. Spreading the space charge over a width Δ acknowledges to a first approximation the effect of diffusion; although, using a δ function for surface charge leads to the same results. The field is assumed small enough so that the additional electrons making up the space charge do not affect τ. The solution of the rate equation has a constant part and an oscillating part of the electron density. The constant part is the equilibrium density and the oscillating part is due to the space charge;

$$n=G\tau-\frac{\sigma E_y^0}{e\Delta}\left[\frac{\tau}{1+i\omega\tau}\right]\exp(i\omega t)\ . \tag{41}$$

As explained in Sec. II, I_{AE} is produced by the action of E_z on the oscillating part of the electron density. A time average over one cycle separates the direct current (per unit width). I assume the conductivity is small enough so that the y and z components of the electric field are $\pi/2$ out of phase—always true at low temperatures.

$$I_{\mathrm{AE}}=\mu\Delta\langle\mathrm{Re}(en)\mathrm{Re}[iE_z^0\exp(i\omega t)]\rangle_t\ . \tag{42}$$

Inserting the solution for n yields

$$I_{\mathrm{AE}}=\frac{\mu\sigma E_y^0E_z^0}{2\omega}\frac{(\omega\tau)^2}{1+(\omega\tau)^2}\ . \tag{43}$$

If the lifetime is long compared to a period, $\tau\gg\omega^{-1}$, then essentially all the electrons of the charge packet remain mobile. The second factor in Eq. (43) is unity, and the current produced is that expected for carriers with mobility μ, namely, equal to Eq. (10) or Eq. (11) when the appropriate expression is substituted for E_y^0 and E_z^0. In the other limit, $\tau\ll\omega^{-1}$, that current is attenuated by $(\omega\tau)^2$. This result is somewhat surprising as the average mobility, determined simply by the fraction of each period on average an electron remains mobile, is $\omega\tau\mu$. The additional factor of $\omega\tau$ is due to a change in the phase relation between the mobile charge and E_z. Recall that I_{AE} is produced by the component of the mobile charge that is in phase with E_z. For small τ, the mobile electrons live only a fraction of a cycle after injection, and since the injection is driven by E_y, the oscillations of the mobile charge lag E_y by $\theta\approx\omega\tau$. The component in phase with E_z is $\sin\theta$ of the mobile fraction hence the additional reduction. Notice that the finite lifetime cannot alter the phase of the total charge—n plus the carriers that left the transport level—which is determined by the potential. Rather, it is the fraction of the charge that is in the transport level and thus mobile that falls out of phase when τ is small. The net effect is to strongly suppress I_{AE} when the lifetime is small. This analysis makes it clear why electrons thermalizing through the conduction band should not produce much signal since for these $\tau\approx10^{-12}$ s and for $\omega\approx10^8\ \mathrm{s}^{-1}$ the factor $(\omega\tau)^2\approx10^{-8}$ overwhelms any reasonable band mobility. At higher temperatures where it is possible for the trapped electrons to be thermally reexcited to the transport level, the above analysis does not hold and one must return to a multiple trapping model.

The above example helps one to understand the effect of the traveling wave when transport takes place in a continuous density of tail states. Since hopping can occur throughout the band tail, there is not a single transport level; rather, each level carries some fraction of the total current. Recall that the space charge packets are formed when the current in the y direction meets the boundaries. The electrons so injected start out distributed among the tail states in proportion to the fraction of the current carried by each energy level; from there they cascade to lower levels. The distance an electron must hop increases lower in the band tail. Thus the average hopping time τ, being exponentially related to the hopping distance, is small for electrons near the band edge and grows rapidly as they fall further into the gap. There will be a particular energy level ε_x where $\omega\tau=1$. ε_x separates the injected electrons into two populations. Those that start out above ε_x will quickly hop down to ε_x contributing little to the signal while in higher levels with small τ even though their mobility might be large. Those that start out below ε_x contribute proportional to the mobilities in those levels, but those mobilities will most likely be much smaller than the mobility at ε_x. The average or drift mobility measured by the experiment is an average of the mobilities of levels below ε_x weighted by the fraction of electrons injected into each level and the mobility at ε_x weighted by the fraction of electrons injected at ε_x and above. Quantitative predictions, however, require computation of these fractions and for that the occupation function is required.

The model solved below allows hops only to lower-energy states—a zero-temperature model. Even with this restriction the problem is complicated because the calculation of transport properties requires not only the distribution in energy but also in space. Solving for both simultaneously is very difficult. However, for the purpose of this investigation, it is sufficient (and much easier) to solve for the occupation function using averages for those quantities that depend on the spatial distance between localized states, such as the hopping time or mobility.

Consider a density of localized states, g_i, that is divided into N slices of equal energy width, $\delta\varepsilon$; the index i begins at 1 for the slice highest in energy. A discrete density of states is used in order to facilitate a numerical solution but N is taken large enough to assure a close approximation to the continuum equations. The following set of rate equations must be solved for the occupation function f_i;

$$\frac{dn_i}{dt}=-f_i g_i\left[\frac{1}{\tau_i^{\rm hop}}+\frac{1}{\tau_i^{\rm rec}}\right]+\frac{(1-f_i)g_i}{N_0}G+\frac{h_i}{e}\nabla\cdot\mathbf{j}+\sum_{j=1}^{i-1}\frac{f_j g_j}{\tau_j^{\rm hop}}\frac{(1-f_i)g_i}{N_{j+1}}\ , \tag{44}$$

where

$$N_i=\sum_{j=i+1}^{N}(1-f_j)g_j \tag{45}$$

is the number of unoccupied states below the ith level. The rate equation for each slice consists of four terms. The first term is the loss of electrons from either hops to lower states ($\tau_i^{\rm hop}$) or recombination ($\tau_i^{\rm rec}$). The second is the generation term which distributes the new electrons among all empty states with equal probability. This avoids a special level at the highest energy in which all the electrons are generated. The third term is the gain and loss of electrons due to the divergence of the traveling wave's electric field, the same as in the single transport level example except for the fact h_i which is the fraction of the current carried by the ith energy slice. The final term is the gain from electrons hopping into the ith slice from above.

To solve the equations, average values of h_i and the lifetimes must be related to the occupation function. Energy loss hopping is exclusively nearest neighbor; the average hopping distance is simply related to the density of available states;

$$r_i\approx N_i^{-1/3}\ . \tag{46}$$

The typical hopping time is then

$$\tau_i^{\rm hop}=\nu_0^{-1}\exp(2r_i/a_i)\ . \tag{47}$$

$5\times10^{12}\ {\rm s}^{-1}$ is used for the attempt to hop frequency ν_0. The localization radius a_i should increase nearer to the mobility edge ε_c, although the results do not depend much on the particular form;

$$a_i=a_0\left[\frac{\varepsilon_c-\varepsilon_i}{75\ {\rm meV}}\right]^{-1/2} \tag{48}$$

is a convenient function using $a_0=14$ Å so that $a_i=7$ Å at the bottom of the band tail.[21]

The recombination lifetime, which for completeness should include both a geminate and nongeminate lifetime, is more troublesome since it depends on the distribution of electron-hole distances. For simplicity, the nongeminate lifetime is calculated using Eq. (47) with the hop distance replaced by half the average distance between holes. The geminate lifetime presents a greater problem since it depends on the distance each electron hops away from its starting point. Since the average hopping distance grows with each hop, the total distance can be approximated by the distance of the last hop. Further, that distance can be approximated by the average distance between states at the energy level into which the electron hopped (at least this forms an upper bound). The geminate lifetime is then calculated from Eq. (47) using this distance. The nongeminate and geminate lifetimes are combined in inverse to give $\tau_i^{\rm rec}$. These approximations are crude (and the price I pay for not solving the spatial problem), but fortunately, $I_{\rm AE}$ turns out to be independent of $\tau_i^{\rm rec}$.

Each energy slice is assigned an average mobility appropriate for transport by the downward hops an electron makes from that slice. It is calculated from the hopping distance and time and the local inverse logarithmic slope of the density of states, ε_0,[22]

$$\mu_i=\frac{er_i^2}{3\tau_i^{\rm hop}\varepsilon_0}\ . \tag{49}$$

The conductivity and h_i of the ith slice follow directly;

$$\sigma_i=ef_i g_i\mu_i \text{ and } h_i=\sigma_i/\sigma\ . \tag{50}$$

Solving the rate equations (44) analytically is difficult because they are nonlinear and all the energy levels are coupled. However, an adequate solution can be obtained numerically in two steps. First the equations are solved without the traveling wave, that is, without the $\nabla\cdot\mathbf{j}$ term, by an iterative procedure to obtain the equilibrium occupation function f_i^0. Then an oscillating solution is added;

$$f_i=f_i^0+A_i\exp(i\omega t)\ , \tag{51}$$

and A_i is obtained by inserting this form into the complete equations (44) and solving assuming A_i is a small perturbation. Figure 7 shows the equilibrium occupation functions obtained for different generation rates. An exponential density of states was used;

$$g_i=g_0\delta\varepsilon\exp(\varepsilon/\varepsilon_0)\ , \tag{52}$$

with $\varepsilon_0=25$ meV and $g_0=4\times10^{21}\ {\rm cm}^{-3}{\rm eV}^{-1}$. The occupation function is as one would expect with the upper states having a very small occupancy, the lower states completely filled, and a pseudo-Fermi level in between. The energy of the pseudo-Fermi level ε_f is determined by the balance between the generation rate and the recombination rate at ε_f—almost all recombination occurs from ε_f.

Figure 8 shows the fraction of the photoconductivity,

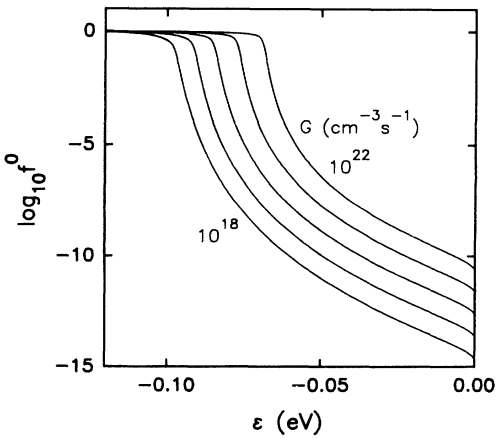

FIG. 7. The equilibrium occupation function for the model described in the text for various generation rates G. G increases from 10^{18} to $10^{22}\ {\rm cm}^{-3}\,{\rm s}^{-1}$ in order of magnitude steps.

TABLE I. The photoconductivity, normalized photoconductivity, and traveling-wave mobility at several generation rates calculated using a model of energy loss hopping through the conduction-band tail.

G ($cm^{-3}s^{-1}$)	σ (S/cm)	σ/eG (cm^2/V)	μ ($cm^2/V\,s$)
10^{18}	8.6×10^{-12}	5.4×10^{-11}	5.2×10^{-4}
10^{19}	8.0×10^{-11}	5.0×10^{-11}	5.7×10^{-4}
10^{20}	7.4×10^{-10}	4.6×10^{-11}	6.3×10^{-4}
10^{21}	6.9×10^{-9}	4.3×10^{-11}	7.0×10^{-4}
10^{22}	6.5×10^{-8}	4.1×10^{-11}	8.0×10^{-4}

h_i, and the fraction of I_{AE} carried by each energy slice for $G=10^{21}$ $cm^{-3}s^{-1}$ normalized to one at the peaks. The dominant contribution to the photoconductivity occurs near ε_f; the numerical results show that h_i is maximum where the occupation function is about 0.1. As expected, the levels near ε_x contribute most to I_{AE}, $\omega\tau=0.4$ at the peak, in spite of the fact that most of the electrons making up the space charge are injected around ε_f as h_i shows. Obviously the traveling-wave experiment measures a special class of carriers different from those responsible for the photoconductivity. Table I lists the calculated values of photoconductivity for various generation rates. The predictions of normalized photoconductivity are close to the values measured for a-Si:H, which are in the range $(1-3)\times10^{-11}$ cm^2 V^{-1}.[19] The exponent γ in the relation between conductivity and generation rate $\sigma\propto G^{\gamma}$ is predicted to be 0.93, also in good agreement with the measured value.[19] The successful photoconductivity calculations indicate that the hop down transport and the occupation function are probably correct at least for the energy levels responsible for the photoconductivity. Table I also lists the mobility calculated from Eq. (12) using the I_{AE} values generated by the model.

This model is valid only for sufficiently low temperatures since hops to higher-energy levels are not considered. Including such up hops would yield the temperature dependence of the mobility at the cost of increased complexity. An argument used by Monroe[23] can estimate the temperature at which the up hops become important and, thus, where the mobility should begin to show a temperature dependence. For a given density of states, there is an energy ε_m at which the average probability to hop to a state lower in energy equals the average probability of thermal excitation to a higher level. Carriers in states lower than this level will most likely be excited upwards, whereas, those in higher levels will hop down. If ε_x lies above ε_m then the carriers contributing to I_{AE} will only hop down, and the low-temperature limit is valid. Conversely, if ε_x lies below ε_m then upward hops are important and the mobility acquires a temperature dependence. For an exponential density of states, ε_m is given by[23]

$$\varepsilon_m=3\varepsilon_0\ln[0.46k_BT/a_0\varepsilon_0(\varepsilon_0g_0)^{1/3}]\ . \tag{53}$$

Setting ε_m equal to the value of ε_x determined by the calculation, 67 meV below ε_c, and using the values for ε_0, g_0, and a_i given above results in a critical temperature of about 120 K. Below this temperature, up hops can be ignored, at least for calculating the direct current, and I_{AE} should be independent of temperature.

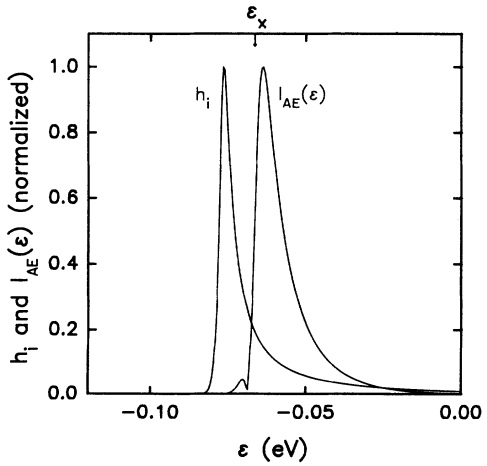

FIG. 8. The relative contribution of each level to the photoconductivity, h_i, and I_{AE} for $G=10^{21}$ $cm^{-3}s^{-1}$. The energy marked ε_x is the level where $\omega\tau=1$.

IV. EXPERIMENTAL DETAILS

Before turning to the data, certain experimental details and the sources of errors need to be discussed. An overview of the apparatus is shown in Fig. 1(b). The heart of the apparatus is a plate of y-z cut $LiNbO_3$. An aluminum interdigital transducer, patterned on the surface, generates a surface acoustic wave propagating along the z axis. $LiNbO_3$ is piezoelectric; thus, associated with the strain of the SAW is precisely the traveling sinusoidal electric potential postulated in the preceding section, Eq. (1). After the SAW travels underneath the sample, it is absorbed by acoustical damping material on the ends of the plate. The transducer also generates a wave in the opposite direction that is immediately absorbed by the damping material. The ends of the plate are angled so that any part of the SAW not absorbed is reflected away from the sample. Care is taken to reduce reflected waves since they interfere with the main SAW and produce aberrant currents in the semiconductor. Since the transducer resonates at a particular frequency measurements can only be made near that frequency for a given plate; most of the data in the following sections are for an 18-MHz transducer.

The sample is supported on the surface of the $LiNbO_3$ by two strips of Kapton along the edge away from the SAW. The Kapton is typically 7 μm thick although the height of the air gap can vary from this value and must be measured each time a sample is placed in position. If the sample need be nearer the surface, the Kapton is eliminated, and the sample is held up by random dust particles. Air gaps produced in this way tend to be about 1 μm though again measurement is necessary. Two clips hold the sample in place. The sample extends beyond the edge of the $LiNbO_3$ to allow leaf springs to make contact with the metal electrodes. The sample is upside down so all connections have to made from below. A thermocouple makes contact with the substrate near but not directly above the active area of the sample. Good thermal contact is assured by placing the junction of the thermocouple in a small puddle of GaIn.

The $LiNbO_3$ rests on a block of copper that has a resistive heater embedded within it which can raise the temperature to 475 K. The block in turn rests on a small hollow stainless steel chamber with external connections to allow cooled air or liquid N_2 to flow through it. In this way the temperature can be cooled below 200 K. Everything is inside a copper can within a vacuum chamber. During measurements dry N_2 flows through the chamber at a pressure of 1 Torr. The N_2 provides the thermal connection between the $LiNbO_3$ and the sample.

The samples are, for the most part, *a*-Si:H prepared by glow-discharge decomposition of SiH_4. The thin films are grown on 1×0.5-in.^{2} pieces of Corning 7059 glass using deposition conditions known to produce high-quality material—low defect density and noncolumnar growth. A typical sample is 1 μm thick and 6 mm wide with 2 mm between the electrodes. Doped material is prepared by adding a certain concentration of either PH_3 or B_2H_6 to the SiH_4; the doping of specific samples mentioned below is the relative gas phase concentration of the doping gas.

A typical experiment on a sample of *a*-Si:H begins by annealing the sample at 450 K. Data are recorded as the temperature falls to room temperature over the course of about three hours. The temperature is then lowered to the lowest value and data are recorded as the sample warms to room temperature. At each measurement temperature, I_{AE} is recorded as well as the voltage necessary to null the current, V_{AE}. From these values and the dimensions of the sample the conductivity is calculated. Also recorded are the frequency, which is varied as the velocity of the SAW changes with temperature shifting the transducer's resonance frequency, and the power absorbed by the transducer from which ϕ_0 is calculated. The mobility can then be calculated using values for ϵ obtained from the literature and h which is measured after the sample is positioned on the plate. The measurement of each value as it relates to possible errors is considered next.

A. Current and voltage

Either a Keithley 610C or 617 electrometer is used to measure the current. The resolution and sensitivity of either electrometer exceed the needs of the experiment. The smallest current capable of being measured, which essentially determines the lowest conductivity a sample may have, depends on the amount of current jitter or anomalous current offset. The main source of the current noise is the $LiNbO_3$. $LiNbO_3$ is both piezoelectric and pyroelectric; mechanical vibrations or temperature changes induce electric fields that are capacitively coupled to the current electrode. A sudden change in pressure or temperature produces transitory currents in excess of 5×10^{-11} A. Smaller fluctuations or drifts, especially in temperature, induce smaller but still significant currents. The problem is troublesome mainly at the lowest temperatures where the temperature regulation is poorest and I_{AE} is small. In general, currents below 5×10^{-13} A cannot be trusted. In a different apparatus designed to allow measurements at liquid-He temperatures, special precautions are taken to limit current jitter to a few femtoamp with a minimum detecable current signal of 10^{-14} A under the best circumstances; the low-temperature apparatus is described below in Sec. VI A.

V_{AE} is determined by applying a voltage to null the current and as such is basically a current measurement limited by the factors discussed above. The smallest V_{AE} is determined by the voltage burden of the electrometer. The manufacturer specifies the voltage burden to be less than 0.1 mV for the 610C and 1 mV for the 617. As V_{AE} approaches these values the current generated by the voltage burden is confused for I_{AE}, making the measurements unreliable. The limit on V_{AE} determines at low temperatures the minimum measurable mobility. As described in the preceding section, V_{AE} also decreases at large conductivities due to the screening of the electric field by the charge. Thus the limit on V_{AE} also determines the maximum conductivity that can be tolerated.

B. The air gap

The strength of the electric field decreases rapidly away from the surface of the $LiNbO_3$, and as a result, I_{AE} depends strongly on the distance h from sample to $LiNbO_3$. For example, changing h from 3 to 4 μm decreases I_{AE} by 25% for a SAW frequency of 18 MHz. Therefore any uncertainty in h leads to a large uncertainty in the mobility.

The air gap is measured interferometrically taking advantage of the fact that h is equal to a small number of wavelengths of visible light. Monochromatic light shining through the air gap creates an interference pattern which reveals the variations in the gap over the area of the sample. The pattern is usually a set of Newton's rings due to curvature of the sample; stress in the *a*-Si:H bends the glass substrate into a convex meniscus. The beam from a He-Ne laser scattering off the roughened bottom of the $LiNbO_3$ provides a convenient source of uniform illumination from below. The interference conditions are the usual ones, $2h\cos\theta=m\lambda$, where constructive interference occurs for integer m and destructive for half integer. From one bright fringe to the next, h changes by $\lambda/2\approx0.32$ μm. The gap is usually smallest near the center.

The interference pattern itself does not determine h since m is not known for the central spot. To determine m either h or λ is varied. Decreasing h by exerting pressure with a sharp probe until the sample contacts the $LiNbO_3$ results in the most accurate measurement. The number of extra fringes that appear as the gap narrows is m. With patience and a steady hand up to 25 fringes can be reliably counted, which corresponds to $h=8$ μm. The error in the measurement is $\frac{1}{4}$ of a fringe or 0.08 μm due to the difficulty of detecting gradations within a light or dark region by eye. Larger gaps can be measured by varying λ; the intensity of the central spot oscillates uniformly as a function of $1/\lambda$ with the spacing between maxima equal to $(2h)^{-1}$. It is feasible to observe the changing pattern by eye using the light from a monochromator. However, the range of λ is restricted at long wavelengths by the sensitivity of the eye to $\lambda<610$ nm and at short wavelengths by absorption in the a-Si:H to $\lambda>490$ nm. In order to have sufficient maxima or minima in this range, h must exceed 5 μm. Also, for h larger than 11 μm, the pattern becomes hard to discern. However, as the observations are quick and convenient, I have used this method to measure air gaps in the range 6–10 μm. Repeating the measurements several times results in a variance typically around 0.8 μm. Alternatively, a far-infrared spectrometer is used to accurately measure the transmission. The copper support block has a 2-mm hole directly under the sample and can be removed from the chamber and mounted in the spectrometer. Very accurate interference oscillations can be obtained for $1.5<\lambda<4$ μm. However, multiple reflections within the thin film of a-Si:H cause an additional interference pattern that tends to obscure the gap's pattern. Reliable peak positions are obtained only if the two patterns oscillate at different frequencies; thus h must be at least twice the optical path length in the a-Si:H. For a typical 1-μm-thick sample h must exceed 7 μm. Based on the quality of a linear regression using all the peaks, I estimate the error to be about 5%.

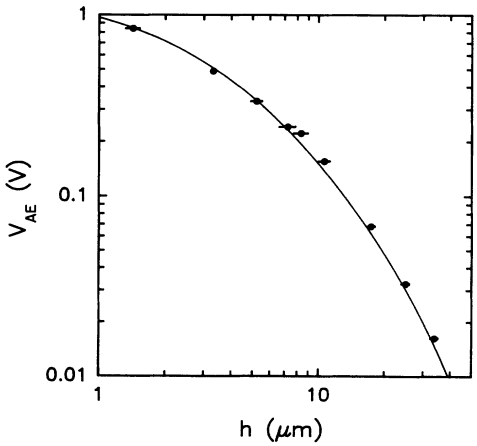

FIG. 9. The dependence of the direct voltage V_{AE} on the spacing between the $LiNbO_3$ and the semiconductor, h. The curve is the prediction of the surface charge theory. The points are measurements with the temperature ($T=27$°C) and SAW power held constant. The sample is n-type a-Si:H (10 ppm PH_3).

In order to test the accuracy of the h measurements, I measured V_{AE} as a function of h keeping all other parameters constant. A sample of n-type a-Si:H was placed on the $LiNbO_3$ using spacers of different thicknesses to obtain gaps from 1.4 to 34 μm. The resulting variation in V_{AE} agrees very well with the surface charge theory, Eqs. (12) and (13), as shown in Fig. 9. The error bars are based on the considerations discussed above. There is one unknown parameter, μ, which controls the vertical position of the line but not the shape; μ has been adjusted to provide the best fit to the data. The good fit demonstrates that h is accurately determined.

The gap is measured immediately after the sample is positioned and again just before it is removed and typically the two measurements agree within error. The interference pattern is occasionally examined during the measurements to determine whether the gap is changing as the apparatus is heated or cooled; no change is observed.

C. The potential at the $LiNbO_3$ surface

The potential at the $LiNbO_3$ surface increases as the square root of the power carried by the SAW, P_{SAW}. The proportionality constant depends on the material and propagation axis; for y-z cut $LiNbO_3$,[24]

$$\phi_0^2=2.10\times10^{10}(\text{cm}\,\Omega\,\text{s}^{-1})\frac{P_{SAW}}{w\omega}\ , \tag{54}$$

where w is the width of the transducer. Since I_{AE} is proportional to ϕ_0^2, any uncertainty in P_{SAW} produces a proportional error in the mobility. The power amplifier that drives the transducer separates and measures the power that is delivered to the transducer and the power that is reflected back to the amplifier. Some fraction of the net absorbed power, P_{net}, is dissipated by resistive losses within the transducer and cable or by generating other types of acoustic waves. Determining these losses leads to the greatest uncertainty in P_{SAW}.

The power of the SAW generated by an interdigital transducer has the frequency dependence of an end-fired antenna array. Since I_{AE} is proportional to P_{SAW}, I_{AE} is a convenient probe of the power actually going into the SAW. Shown in Fig. 10(a) is the resonance as detected by I_{AE} as well as P_{net}. Between the main resonance and the side lobes, I_{AE} dips to zero, indicating that no SAW is present at these frequencies. Nevertheless a significant amount of power is absorbed which must be due to various losses. Interpolating between these frequencies yields the loss at the operating frequency with an error of about 5%. It may be the case that the resonance affects the loss mechanisms so that a simple interpolation is not correct. For example, the impedance of the transducer varies greatly through the resonance and the currents in the transducer and thus the resistive losses also change. To test this and determine if any other systematic problems exist in the power calculations, the mobility is calculated from the data in Fig. 10(a) throughout the resonance, not

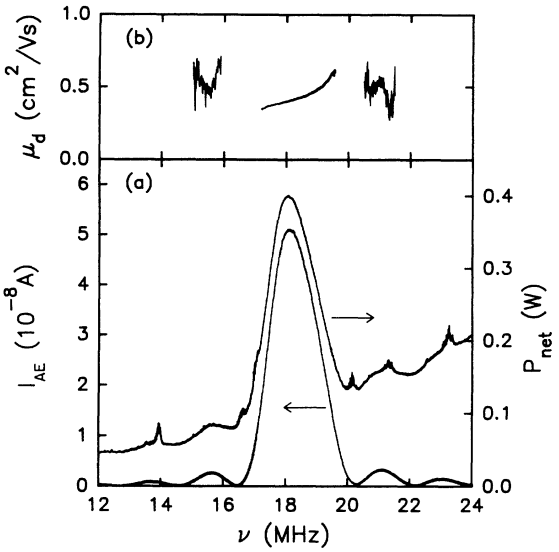

FIG. 10. (a) The frequency dependence of I_{AE} and the net power delivered by the amplifier, P_{net}, around the primary resonant frequency of the transducer. The sample is n-type a:Si:H (100 ppm PH_3). (b) The mobility calculated from the data in (a) for the central part of the main resonance and the nearest side lobes.

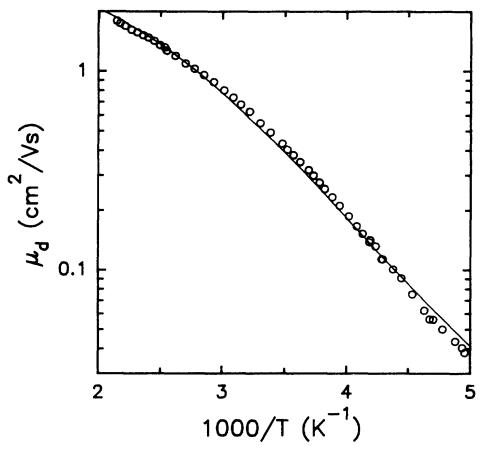

FIG. 11. The temperature dependence of the drift mobility of n-type a-Si:H (30 ppm PH_3). The line is a fit to the data based on a multiple trapping model.

just at the peak. If the losses are calculated correctly the mobility should be constant. (The mobility itself depends negligibly on frequency over the region of the resonance). As Fig. 10(b) shows, the calculated mobility does vary about 25% about the mean over the main resonance indicating some residual and systematic difficulty in determining P_{SAW}. The variance is small considering that the power varies by a factor of 5 over the same region. Nevertheless, the absolute mobility values are uncertain to this degree. Since measurements are always made at the peak frequency, the same error is made for all measurements; this systematic uncertainty does not affect relative comparisons of the mobility at different temperatures or from sample to sample but must be considered when comparing with values measured by different apparatus or techniques. Note that the small sharp peaks that appear in P_{net} at various frequencies are due to resonances between the top and bottom of the plate. Should one of these occur at the operating frequency, P_{SAW} would be overestimated, resulting in an anomalous small mobility. Such bulk resonances can be shifted by removing some material from the bottom of the plate.

V. HIGH-TEMPERATURE DATA AND ANALYSIS

The following are several examples of traveling-wave drift-mobility measurements and the information that can be extracted from the data. All measurements used an 18-MHz SAW with $P_{SAW} \approx 0.15$ W.

A. Temperature dependence of the drift mobility

The drift mobility of n-type a-Si:H (30 ppm PH_3) obtained from traveling-wave data is shown in Fig. 11. The temperature dependence is similar to that seen by TOF in undoped a-Si:H in that the mobility is activated at lower temperatures with an activation energy of 0.15 eV and falls below the Arrhenius line above room temperatures. However, the values are a factor of 2 less than those of undoped material, which is an effect of the doping.[14,25] The conductivity of the sample ranges from 7×10^{-5} S cm^{-1} at 200 K to 3×10^{-2} S cm^{-1} at 450 K. For $T>240$ K, the conductivity exceeds 4×10^{-4} S cm^{-1}, and the current at the far surface is screened, as discussed in Sec. II A. Throughout most of the temperature range studied, the mobility reflects carriers within a diffusion length of the free surface. V_{AE} is negative indicating electron dominated conduction as expected for an n-type semiconductor.

Also shown in Fig. 11 is a fit to the data evaluated from the multiple trapping model, Eq. (36), using an exponential DOS;

$$g(\varepsilon)=g_c\exp[(\varepsilon-\varepsilon_c)/\varepsilon_0] \ . \tag{55}$$

The fitting parameters are $\varepsilon_0=25$ meV and $\mu_0=5$ cm^2 V^{-1} s^{-1}. The theoretical curve reproduces the data quite well although there are small systematic deviations. Demanding a better fit would necessitate deviations from a purely exponential DOS, which many workers in the field believe to be the case. Including a linear region near the mobility edge or other features would allow for a better fit. However, it makes little sense to try for this level of accuracy based solely on the drift-mobility data since the calculation assumes that the band mobility and DOS are temperature independent. There is no direct measurement of the temperature variations of μ_0; however, theoretical models have predicted $\mu_0 \propto T^{-1}$.[26] The freedom afforded by allowing μ_0 to vary allows good fits to the data for most of the proposed DOS functions. In addition, it is possible that the density of band-tail states changes significantly with temperature. Recent results from photoelectron spectroscopy indicate that the conduction-band tail is exponential but broadens from $\varepsilon_0=40$ meV at room temperature to $\varepsilon_0=60$ meV at 500

K for n-type a-Si:H[27] Although it is meaningless to try to derive a DOS that varies with temperature from the data in Fig. 11, the photoelectron DOS can be used as input to the model. The calculated mobilities are then found to be consistent with the measured values,[28] providing the band mobility is about 50 $cm^2 V^{-1} s^{-1}$. The large μ_0 is required because of the large number of traps implied by a broader tail.

B. Uniformity of drift mobility throughout the semiconductor

At the end of Sec. II A, I noted that the suppression of the far-surface current once the conductivity exceeds 4×10^{-4} S cm^{-1} (for 18 MHz) allows a sensitive test for any difference between the drift mobility at the near and far surfaces. The idea is that any difference upsets the near cancellation of the two surface currents for conductivities less than the critical value leading to erroneous mobility values. However, above the critical value, only the current at the near surface is present and then the drift mobility at the near surface is correctly calculated from the data. Any unusual jump in the measured mobility as the conductivity sweeps through the critical value is evidence that the drift mobility is different at each surface.

A sample of n-type a-Si:H (100 ppm PH_3) was subjected to a series of one-hour, high-temperature annealings at progessively higher temperatures starting at 550 K. The drift mobility was measured after each anneal; the values obtained before annealing, after the 630-K anneal, and after the 730-K anneal are shown in Fig. 12. As hydrogen is driven out of the a-Si:H, the drift mobility and the conductivity decrease substantially. The temperature at which the conductivity reaches 4×10^{-4} S cm^{-1} shifts upward and is marked by an arrow for each curve. It is precisely at these temperatures that the drift mobility of the lower two data sets appears to have anomalous curvature. The fact that the mobility at lower temperatures lies above the extrapolation of the higher-temperature points indicates that the current at the far surface is suppressed.

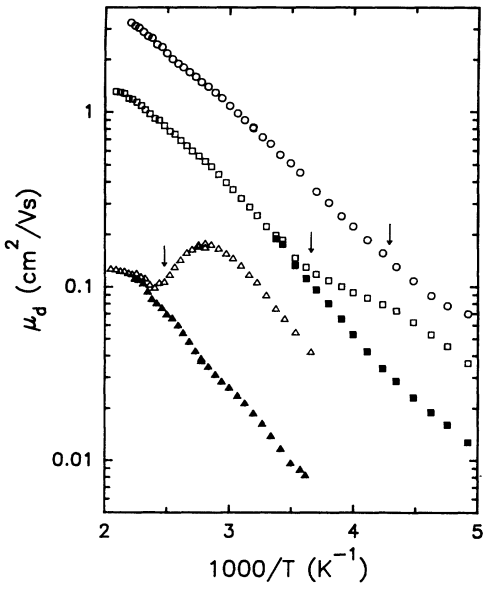

FIG. 12. The drift mobility of n-type a-Si:H (100 ppm PH_3) as deposited (circles), after one hour at 630 K (squares), and after one hour at 730 K (triangles). The closed symbols are obtained by correcting the original data to take into account a lower mobility at the semiconductor-substrate interface as described in the text. The arrows indicate the temperature at which the conductivity reaches 4×10^{-4} S cm^{-1}.

The factor by which the mobility differs at the two surfaces can be obtained from the data. Let the drift mobility at the near (1) and far (2) surfaces be in the ratio $R_\mu=\mu_2/\mu_1$, and let $R_I=(I_1+I_2)/I_1$; R_I is the quantity graphed in Fig. 2 and is a measure of how closely the two currents cancel when the mobility is the same at each surface. The observed mobility μ_{eff} is related to μ_1 by

$$\mu_1=\frac{R_I}{1-R_\mu+R_\mu R_I}\mu_{\text{eff}} . \tag{56}$$

Corrections are applied to the data using Eq. (56) by treating R_μ as a variable parameter and searching for a value that eliminates the anomalous curvature around the critical conductivity. The closed symbols of Fig. 12 are the corrected data using R_μ values of 0.85 and 0.60 for the 630- and 730-K anneals, respectively. This substantial decrease of the far-surface drift mobility may be caused by the accumulation of hydrogen at the semiconductor-substrate interface. Samples of a-Si:H made under conditions that incorporate excess amounts of hydrogen are known to have broader band tails, which would lower the drift mobility.[29]

C. Drift mobility of rapidly quenched a-Si:H

The electronic configuration of a-Si:H evolves with temperature, and the rate at which the configuration approaches an equilibrium depends strongly on temperature in a way reminiscent of the structural relaxation in a glass.[30] Just like a glass, quenching a sample can preserve the high-temperature electronic configuration below the temperature T_E at which the relaxation proceeds on a laboratory time scale. The effect is seen in a variety of measurements; for example, a rapidly quenched n-type sample has three to five times the conductivity of the same sample slowly cooled.[31] Street *et al.* have proposed that the main effect is an increase in the doping efficiency at higher temperatures mediated by diffusing hydrogen.[30]

A sample of n-type a-Si:H (100 ppm PH_3) was quenched by dropping into liquid N_2 directly from a furnace after being annealed in an atmosphere of dry N_2 at 450 K; the sample completely cooled within one second. After warming to room temperature in dry N_2, the sample was placed in the traveling-wave apparatus, and the conductivity and drift mobility were measured from 200 to 450 K. After annealing at 450 K for more than one hour, measurements were made while the sample slowly cooled to 315 K over the course of several hours. The sample was then cooled to 200 K and the measurements were completed as the sample warmed to 315 K.

The conductivity of the quenched state below $T_E = 390$ K is almost three times that of the slowly cooled state, whereas μ_d is nearly, but not quite, the same in both states (Fig. 13). Above 300 K and below T_E, μ_d of the quenched state is 10% larger, but below 250 K it is smaller by about 20%. Since the sample is measured in both states without repositioning and with the same SAW power and frequency, systematic errors due to uncertainties in h and P_{SAW} are the same for all points. The relative changes in μ_d that are observed are, therefore, accurate to within the error in the current and temperature—a few percent—providing no spurious currents are present, a possibility at the lower temperatures arising from temperature changes of the $LiNbO_3$. The fact that quenching does not decrease μ_d at intermediate temperatures indicates that if the conduction-band tail broadens with temperature as reported in Ref. 27 then a broader band tail is not frozen in by the quenching; the mechanism that governs the broadening is different from that of the dopant-defect equilibration.

The enhancement of μ_d above 300 K is likely due to an increase of the Fermi level in the quenched state.[32] As the Fermi level moves toward the band edge, formerly empty localized states become filled with equilibrium carriers and can no longer act as traps for the carriers in the charge wave, and fewer traps cause μ_d to increase. The relative increase in μ_d can be related to the number of traps lost and, therefore, to the density of states at the Fermi energy. Let the drift mobility of the quenched state be x times that of the slowly cooled state. From Eqs. (36) and (37), x can be related to the occupation function $A(\varepsilon)$ for a small increase of the Fermi level $\delta\varepsilon_f$:

$$\frac{(x-1)\mu_0}{x\mu_d} = -\int^{\varepsilon_c} \frac{g(\varepsilon)}{N_c} \frac{\partial A(\varepsilon,\varepsilon_F)}{\partial \varepsilon_F} \delta\varepsilon_F d\varepsilon \ . \tag{57}$$

The derivative of $A(\varepsilon)$ is very strongly peaked at the Fermi energy, so the DOS function can be replaced by its value at ε_F. This may seem a bad approximation since the DOS may also be a strong function of energy. But the derivative decreases exponentially above ε_F with a logarithmic slope of $2/k_BT$, and even an exponential DOS would need ε_0 less than 20 meV to introduce significant error at 350 K. The remaining integral can be solved analytically if the imaginary term in Eq. (34) is ignored, which is valid when the demarcation energy, Eq. (38), lies below ε_F. The resulting expression provides an interesting connection between the mobility and the DOS at the Fermi energy;

$$\frac{(x-1)\mu_0}{x\mu_d} = \frac{g(\varepsilon_F)\delta\varepsilon_F}{N_c} \exp[(\varepsilon_c - \varepsilon_F)/k_BT] \ . \tag{58}$$

The Fermi energy at 350 K obtained from the conductivity assuming a prefactor of 200 $S\,cm^{-1}$ is 0.31 eV below the mobility edge. $\delta\varepsilon_F$ is simply related to the ratio of conductivities in the quenched and slowly cooled states; $\delta\varepsilon_F = k_BT \ln(\sigma_q/\sigma_{sc}) = 24$ meV. g_c obtained from photoemission is about 4×10^{21} $cm^{-3}eV^{-1}$ (recall $N_c = k_BTg_c$).[33] x and μ_d at 350 K are 1.1 and 1 $cm^2V^{-1}s^{-1}$, respectively. Inserting these values into Eq. (58) yields

$$g(\varepsilon_F) \approx 1.6\times10^{16} \left[\frac{\text{V s}}{\text{cm}^5\,\text{eV}}\right] \mu_0 \ . \tag{59}$$

The density of states 0.31 eV below the mobility edge is unlikely to exceed 3×10^{17} cm^{-3} eV^{-1}, at least for the popular models of the band tail, which constrains the band mobility to no more than 20 $cm^2V^{-1}s^{-1}$. If the very broad band tails seen by the photoemission experiment are correct then a larger μ_0 would again be necessary.

Changes in the Fermi level will not affect μ_d if the demarcation level lies above ε_F. As the temperature decreases, ε_d moves upward and, at a certain temperature, passes through ε_F. The mobilities in the two states should then merge together; this occurs at 300 K. By setting ε_d equal to ε_F, one can solve for the remaining variable, ν_n, which works out to 4×10^{12} s^{-1}, a reasonable value for a phonon-mediated attempt-to-escape frequency.

The data at lower temperatures are more difficult to explain. A decrease of μ_d usually indicates an increase in the density of trapping states. Quenched a-Si:H contains more active dopants as well as more defects. The defects lie below the Fermi level and should not act as traps. The donor levels are believed to lie within 0.1 eV of the mobility edge and can trap carriers; however, the density of band-tail states is very large at these energies and should render any change in the number of donor states insignificant. More work is needed on this point.

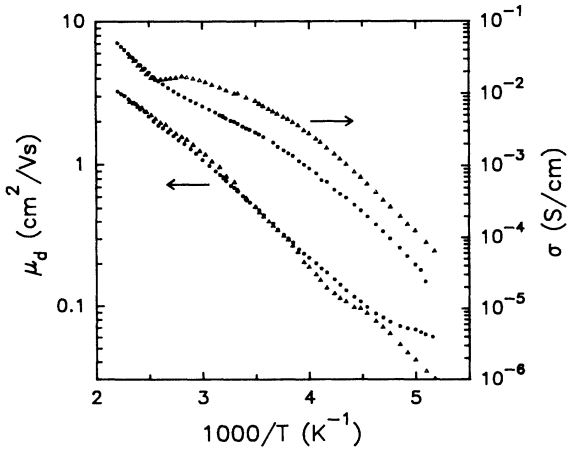

FIG. 13. The temperature dependence of the conductivity and the drift mobility of n-type a-Si:H (100 ppm PH_3) in the quenched state (triangles) and the slowly cooled state (circles).

VI. LOW-TEMPERATURE EXPERIMENTAL DETAILS, DATA, AND ANALYSIS

A. Experimental details unique to low temperatures

In order to permit measurements at lower temperatures, the $LiNbO_3$ is secured to a cold finger thermally

connected to a cryogenic reservoir in a liquid-He Dewar. With liquid H_2 in the reservoir—liquid H_2 is used rather than liquid He because of its much larger heat of vaporization—stable temperatures can be achieved down to 35 K. The temperature is measured by a silicon diode thermometer attached to the back of the substrate with GaIn. Several Torr of He is maintained in the Dewar to provide thermal contact between the sample and the $LiNbO_3$ across the gap. To achieve lower temperatures, the cryogen is filled directly into the Dewar. Liquid H_2 is used for 20 K; the Dewar is filled above the bottom of the copper block but below the sample. Measurements with the sample in liquid H_2 are impossible because the boiling H_2 shakes the piezoelectric $LiNbO_3$ plate causing severe noise. Temperatures from 4 to 1.6 K are obtained with the sample immersed in liquid He; the noise induced by the fine bubbles of boiling He is much less than by boiling H_2. Below the λ point at 2.2 K, there are, of course, no bubbles, and the noise level is greatly reduced. Data between 4 and 20 K and between 20 and 35 K are difficult to obtain because the large amount of power dissipated by the SAW and the illumination causes rapid warming. Measurements made while warming through these temperature ranges suffer from excess noise. The semiconductor is continuously illuminated by a focused 75-W arc lamp shining through the substrate. For most measurements, filters remove photons below 1.5 and above 2.35 eV. The absorbed photon flux for a-Si:H is typically 5×10^{17} $cm^{-2}s^{-1}$ resulting in photoconductivities of about 5×10^{-9} $S\,cm^{-1}$ at liquid-He temperatures.

In order to increase the sensitivity as well as limit spurious signals, two SAW transducers are used, one on each side of the sample. By alternately exciting one then the other transducer, the direction of the SAW traveling beneath the sample is reversed thereby changing the sign of I_{AE}. The current difference is then used to calculate the mobility. Not only is the signal thereby twice as large but spurious signals, such as a photovoltage or thermovoltage or electrometer drift, that do not depend on the direction of the SAW are eliminated by the subtraction. The current is recorded on a strip chart; a typical run is shown in Fig. 14. Notice that without a SAW there is still a photoinduced current that would confound the measurement if a single transducer were used. Most of the samples display photovoltages at low temperatures, and some are larger than the band gap; the phenomenon is not well understood.[34] However, the photovoltages are not correlated with I_{AE}.

The same sources of systematic error present at higher temperatures, uncertainty in h and P_{SAW}, afflict the low-temperature measurements. In addition, current fluctuations are more important because the currents are much smaller. Typically for a-Si:H at low temperatures, V_{AE} ranges from several tenths of a volt to several millivolt, which requires a sensitivity of a picoamp down to several tens of femtoamp. The amount of current noise encountered varies depending on the temperature, the light intensity, and P_{SAW}. With the sample in superfluid liquid He, the noise is typically several femtoamp. At any higher temperature, the fluctuations are larger:

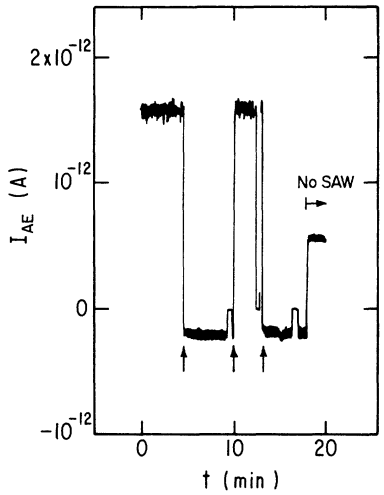

FIG. 14. A strip chart recording of I_{AE} for a sample of intrinsic a-Si:H immersed in liquid He at 4 K. The direction of the SAW is reversed at the times indicated by the arrows. The sample's conductance is 3.4×10^{-12} $S\,cm^{-1}$ and $P_{SAW}=0.35$ W. The SAW is turned off at the end; the residual current is due to a photovoltage. The recorder is zeroed at three times while 10 V is applied to measure the conductance.

$(0.5-1)\times10^{-13}$ A at 4 K, due principally to conductance fluctuations caused by the He bubbles scattering the light, and $(1-3)\times10^{-14}$ A at 40 K. On some occasions, long-term drifts are present that may be due to slow temperature changes. Actual errors can be estimated from repeated measurement of the same sample as can be seen in the figures.

B. Data

Data from several samples of a-Si:H demonstrate the unusual temperature dependence of V_{AE} seen at low temperature (Figs. 15 and 16). The data are presented as mobilities calculated using Eq. (12) in order to factor out variations of the gap and SAW power. However, there is doubt as to whether the signal observed at low temperatures can truly be converted to a drift mobility; the quandary is discussed below. Therefore it is more accurate to regard the mobility as simply a normalized V_{AE}. In any case, the data present several interesting features. Above 150 K the drift mobility—and here I can correctly write mobility—agrees with the predictions of multiple trapping theories. Further, the sign of V_{AE} is as expected from the doping—negative for the intrinsic and n-type samples indicating electron conduction and positive for the p-type sample indicating holes. As the temperature is lowered, a minimum occurs near 100 K, and then the mobility rises roughly as $1/T$ until it flattens off at the lowest temperatures reaching a value 30–50 times that at the minimum. V_{AE} of p-type samples, instead of reaching a minimum at 100 K, actually goes through zero and becomes negative somewhere between 40 and 170 K, the signal being too small to measure in this range. All samples yield the same sign below 100 K regardless of the

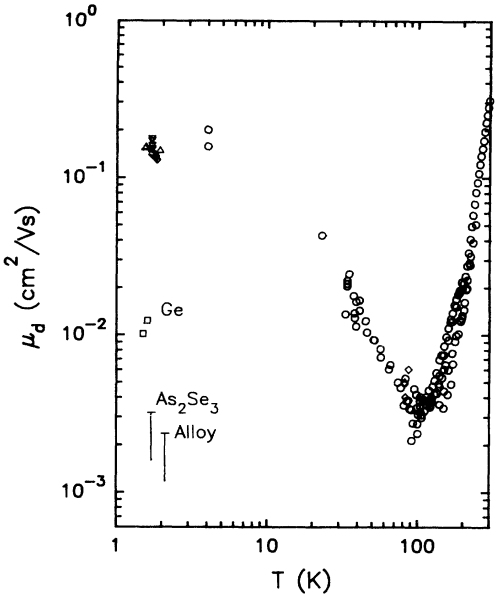

FIG. 15. The traveling-wave mobility of a-Si:H and some other amorphous semiconductors. The circles are for a sample of n-type a-Si:H (800 ppm PH_3). The cluster of points at 1.6 K contains measurements of n-type a-Si:H with different levels of doping: lozenge, 1 ppm; downward triangle, 20 ppm; upward triangle, 1%. The square points are for a sample of evaporated Ge. Samples of evaporated As_2Se_3 and the chalcogenide alloy $As_{35}Te_{28}S_{21}Ge_{15}Se_1$ failed to give a signal; the upper limits for the mobility are shown.

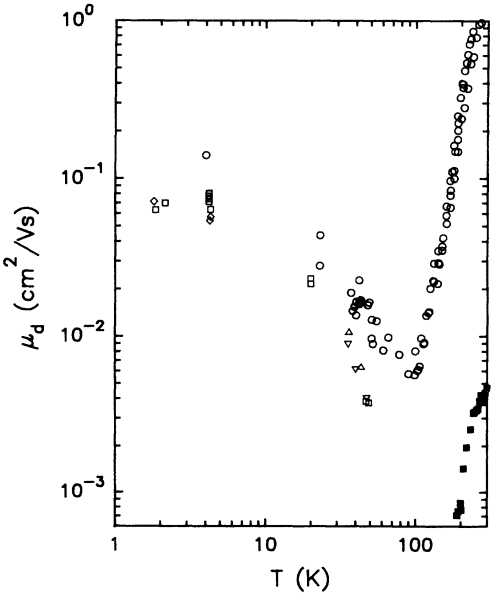

FIG. 16. The traveling-wave mobility of several samples of a-Si:H with different dopings: circle, intrinsic; square, upward and downward triangle, 100 ppm B_2H_6; lozenge, 1% B_2H_6. V_{AE} is positive for p-type a-Si:H at high temperatures indicating hole conduction (closed squares) and is negative everywhere else (open symbols).

doping. The magnitude of V_{AE} depends on the type of doping with p-type a-Si:H giving a signal about a factor of 2 below the n-type and intrinsic material. However, the amount of doping seems to have little effect as demonstrated by the cluster of points at 1.6 K in Fig. 15 that come from samples where the doping is changed by four orders of magnitude. One point is very clear—the values of μ at the lowest temperatures are much larger than those predicted by the theory of the preceding section and listed in Table I. Initially, we suspected that the ac conductivity is much larger than the dc conductivity at low temperatures causing a spurious enhancement of the mobility (as explained in Sec. II).[35] However, subsequent measurements showed that the ac conductivity is only three times the dc value.[36]

As the illumination is reduced by a factor of 10, no change is observed in V_{AE} (Fig. 17). Likewise, there is no systematic change in V_{AE} if filters passing different energy bands of light are used; blue light and red light produce roughly the same signal. Both observations are consistent with the idea that the experiment is probing a special class of carriers. Changing the generation rate moves the position of the pseudo-Fermi level, altering the mobility of those carriers contributing to the photoconductivity. However, unless ε_f nears ε_x, the traveling-wave mobility should remain the same. Likewise, the initial energy of the photoexcited electron is immaterial to transport at ε_x. This would not be so if the transport were taking place while the hot electrons thermalize through the conduction band.

To test whether the observed signal is general to amorphous semiconductors, several samples of material different from a-Si:H were also studied. Two chalcogenide samples—evaporated As_2Se_3 and the alloy $As_{35}Te_{28}S_{21}Ge_{15}Se_1$—failed to give any signal at 1.6 K; the detection limits are shown in Fig. 15. A sample of evaporated Ge did produce a small signal of 10^{-2} cm^2 V^{-1} s^{-1}, also shown in Fig. 15, which is about three

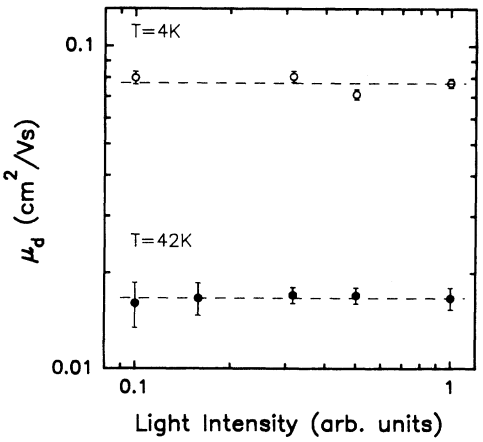

FIG. 17. The invariance of the mobility as the light intensity is varied by a factor of 10 at $T=4$ K (open circles) and $T=42$ K (closed circles). The dashed lines are the average of each set of values. The samples are p-type a-Si:H (100 ppm B_2H_6) and intrinsic a-Si:H, 4- and 42-K points, respectively.

times the noise level. These amorphous semiconductors have a smaller normalized photoconductivity than *a*-Si:H. The smaller bandgap of *a*-Ge compensates for this by absorbing a larger number of photons resulting in a photoconductivity larger than that of *a*-Si:H for the lamp used in the experiment, about 9×10^{-9} S cm^{-1}. The photoconductivity of the alloy is 9×10^{-10} S cm^{-1} and of the As_2Se_3 is 2×10^{-10} S cm^{-1}. However, the smaller photoconductivity clearly does not explain the lack of any signal from the chalcogenide samples since reducing the photoconductivity of *a*-Si:H by using weaker light does not affect the mobility.

The dependence of V_{AE} on the SAW power differs at low temperatures from the strictly linear behavior expected and observed in the multiple trapping region. The SAW power can be varied only by about a factor of 5, but over this range V_{AE} varies superlinearly with P_{SAW} (Fig. 18). Since V_{AE}/P_{SAW} is plotted in Fig. 18, the y intercepts give the term in an expansion of V_{AE} linear in P_{SAW} and the finite slopes indicate a nonzero quadratic term. At 40 and 50 K, the intercept is zero to within error; V_{AE} has a small or no linear component. As a consequence, the data of Figs. 15 and 16 depend on the SAW power in this temperature range and probably up to the minimum at 100 K. (All points plotted in the figures were obtained using $P_{SAW}=0.5$ W.) In contrast, there is a substantial linear component at liquid-He temperatures as well as a quadratic term. A nonlinear dependence of V_{AE} on P_{SAW} may indicate that the nonlinear term of Eq. (2), which was neglected in solving for the potential, becomes important. Including the nonlinear term results in harmonics of the fundamental frequency, and each harmonic produces a direct current via the nonlinear interaction in the same way as the fundamental. If the mobility depends on frequency then V_{AE}/P_{SAW} will vary as the relative strength of the harmonics to the fundamental changes with P_{SAW}. V_{AE} does depend linearly on frequency (Fig. 19), and if the higher harmonics are enhanced with increasing P_{SAW} then V_{AE} will increase superlinearly. However, the lack of a linear term at 40 K but a finite linear term at 4 K is difficult to explain in this way. The nonlinearity could also result if the transport is intrinsically nonlinear in the field. Other probes of transport in *a*-Si:H do show nonlinearities at low temperatures. The photoconductivity of *a*-Si:H becomes super-Ohmic for fields greater than 6×10^4 V cm^{-1}.[37] It was recently observed that the TOF collection efficiency at low temperatures increases rapidly around 2×10^5 V cm^{-1} from a few percent at lower fields to over 80%.[38] However, the maximum electric field in the traveling-wave experiment is much less than these values—about 250 V cm^{-1}. Another possibility is that the anomalous effect to be discussed below is also responsible for the nonlinear dependence on P_{SAW}.

We also investigated the dependence of V_{AE} on the frequency of the surface acoustic wave.[39] Since the transducers generate a surface acoustic wave only in a narrow resonance about a central frequency, different transducers must be fabricated on different plates of $LiNbO_3$ for each frequency studied. Figure 19 shows the temperature dependence of μ calculated from V_{AE} at three frequencies, 20, 39.5, and 60 MHz, for a sample of lightly doped

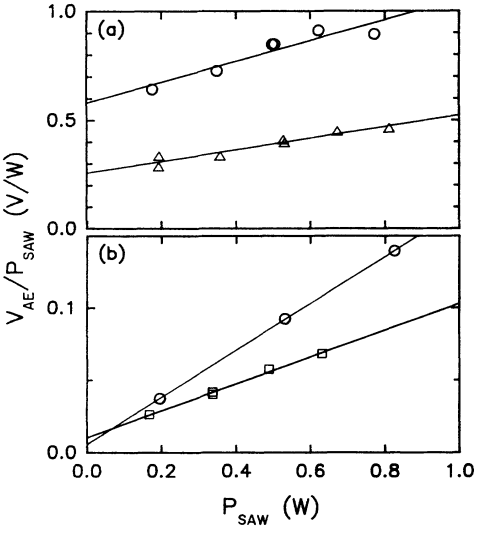

FIG. 18. The dependence of V_{AE} on P_{SAW} for *n*-type *a*-Si:H (800 ppm PH_3) (circles), intrinsic *a*-Si:H (squares), and *p*-type *a*-Si:H (100 ppm B_2H_6) (triangles). The temperatures are (a) 4 K, and (b) 38 and 53 K for the *n*-type and intrinsic samples, respectively. The lines are linear regressions of the data.

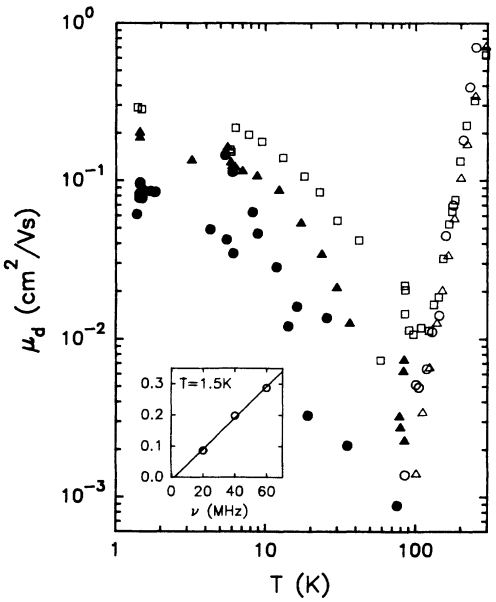

FIG. 19. The traveling-wave mobility of *n*-type *a*-Si:H (1 ppm PH_3) at three SAW frequencies—20 (circles), 40 (triangles), and 60 MHz (squares). The open symbols indicate V_{AE} is negative, and the closed symbols indicate V_{AE} is positive. The sign of V_{AE} above 100 K is always negative as expected for an electron dominated semiconductor, whereas below 100 K the sign depends on the orientation of the y axis of the $LiNbO_3$ plate. The plate used for the 60-MHz measurements is polished on the $+y$ face, whereas the other two plates, used for the lower frequencies, are polished on the $-y$ face. The inset graph shows the frequency dependence of the mobility at 1.5 K; the line is the linear regression of the three points.

n-type a-Si:H (1 ppm PH_3). In the multiple trapping region above 100 K, μ is essentially independent of frequency within the range we investigated, whereas below 100 K, μ increases roughly linearly with frequency. In contrast to the data of Figs. 15 and 16 where the temperature was stabilized for each point the data of Fig. 19 between 5 and 100 K were taken while the sample was warming. This leads to a much greater amount of noise as evidenced by the scatter of the 20-MHz data. The temperature at 1.6 K is, of course, stable, and the data there are much more reliable for determining the frequency dependence, which is shown in the inset. A linear increase of μ with frequency means that V_{AE} increases as the third power of frequency for a constant ϕ_0. Thus the 60-MHz data represent considerably stronger signals and have much less scatter.

During the course of these latter experiments we discovered the anomaly alluded to above—the sign of V_{AE} below 100 K is sometimes positive and sometimes negative depending on the piece of $LiNbO_3$ used. A given plate of $LiNbO_3$ consistently produces the same sign for all samples in the low-temperature region. However, two apparently identical plates of $LiNbO_3$ used to measure the same sample under identical conditions yield signals of the same magnitude but opposite sign. In contrast to the low-temperature behavior, the sign of V_{AE} above 100 K is not affected by which plate of $LiNbO_3$ is used and is entirely consistent with what we expect the dominant carrier to be. We would not have discovered this anomaly had we not been forced to use different plates for the different frequencies.

Clearly the plates cannot be truly identical. The manufacturer cuts and polishes the $LiNbO_3$ along specific directions designated as y-z cut. $LiNbO_3$ is a trigonal crystal with the $3m$ point group (see Weis and Gaylord[40] for a discussion of the crystal structure of $LiNbO_3$). Thus it has a threefold rotation axis (the c axis) and three equivalent mirror planes that intersect the c axis. The Cartesian coordinates are chosen so that the z axis is parallel to the c axis and the y axis lies in one of the mirror planes. A crystal is y-z cut when the long axis of the plate, which is the propagation axis of the surface acoustic wave, is the z axis of the crystal and the y axis is perpendicular to the surface of the plate. X-ray diffraction confirmed that all the plates are oriented correctly. However, $LiNbO_3$ is not symmetric with respect to inversion about the y axis; pressure applied along the y axis produces a polarization that establishes the positive direction of the axis. It turns out that some of our plates have the positive y axis directed out of the polished face ($+y$ face) and some have it directed into the polished face ($-y$ face). And all the plates with a $+y$ face produce a negative V_{AE} for a $+z$ propagating SAW at low temperatures which we normally would interpret as due to electrons and the plates with the other orientation give the opposite sign. In all, seven plates were tested, three with the $+y$ face and four with the $-y$ face polished; thus there is only a 1 in 128 chance that the observed correlation between y-axis orientation and sign of the signal is accidental.

According to the theory developed in the previous sections, the sign of V_{AE} should depend on the sign of the carrier, not the orientation of the $LiNbO_3$. Our chief concern is that the sign anomaly indicates that the signal is not due to the interaction of the traveling electric field with the carriers in the semiconductor but has some other spurious origin. Several tests prove that the interaction is normal in all respects other than the sign. First, the lack of any signal from As_2Se_3 immediately rules out any source of an extraneous signal that does not involve the semiconductor. In particular, capacitive coupling of the electrodes to the $LiNbO_3$ could produce long-lived transient currents if the $LiNbO_3$ is slowly strained, say by the heat dissipated in the damping material. But such currents would be present for all samples or even a substrate with electrodes but no semiconductor. Capacitive pickup is also excluded by an additional test where the voltage lead is left open during the measurement. The true I_{AE} obviously requires a complete circuit through both electrodes in order to flow. However, if the current is capacitively induced then the circuit is completed through the capacitor and the same or larger current would flow with only the electrometer electrode connected. As expected, only short-lived transients are observed with the voltage electrode floating. Another possible source of spurious direct currents is rectification at the metal-semiconductor junction. A particular feature of the real acousto-electric interaction is that current is generated along the whole length of the semiconductor and, as a consequence, I_{AE} is independent of the distance between the electrodes. However, if the current is generated only at the electrodes the bulk of the semiconductor acts as a load resistor; increasing the electrode spacing should then decrease the current. A sample of a-Si:H was measured with electrode spacings of 10, 6, and 2 mm. I_{AE} varied by 10% about the mean of the measurements which is within the uncertainty and much less than the factor of 5 expected if the contacts generate the current. Further, no sign of non-Ohmicity was observed in the current-voltage relation of any sample at low temperatures up to fields of 500 $V\,cm^{-1}$. Another possibility I consider is that the SAW is not a plane wave, Eq. (1), but contains harmonics or other distortions that become important at low temperatures and that may depend on the orientation of the $LiNbO_3$. A simple test for this is the dependence of V_{AE} on the gap, h. Since each Fourier component of the electric potential decreases away from the $LiNbO_3$ surface with a different decay length, the decrease of V_{AE} with h is characteristic of the frequency most important for producing the signal. V_{AE} was determined for three values of h for a sample of a-Si:H under otherwise identical conditions at 1.6 K (Fig. 20). The values agree with the prediction of the surface charge theory for the fundamental frequency of 18 MHz. The first harmonic and subharmonic are clearly excluded. From these results I conclude that the signal produced by the experiment is real in the sense of being due to an interaction of the traveling electric field with the charge carriers of the semiconductor.

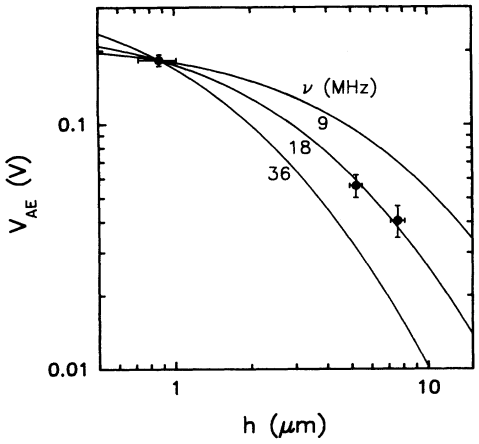

FIG. 20. The dependence of V_{AE} on the gap h, at $T=1.6$ K. The points are measurements using a SAW frequency of 18 MHz. The sample is n-type a-Si:H (20 ppm PH_3). The curves are the expected dependence for 9, 18, and 36 MHz as indicated. The curves have been normalized to the first data point.

C. Discussion of the low-temperature data

Unfortunately, the sign anomaly limits the conclusions that can be drawn from the data. The anomaly itself indicates that the potential at the surface of the $LiNbO_3$ must be more complicated than a traveling plane wave, Eq. (1), and in particular, a heretofore unknown component of the potential that depends on the orientation of the y axis must exist. The articles and texts that derive the surface potential for a Rayleigh wave from the coupled electric-elastic equations result in Eq. (1).[24] Until a complete solution for the potential is formulated, it is not clear how the data below 100 K relate to the transport properties of the semiconductor as Eq. (12) may not be appropriate to calculate a mobility. It cannot even be determined whether the observed temperature dependence is due to changes in the transport or changes in the potential.

Since the data presented in Figs. 15 and 16 cannot accurately be interpreted as the drift mobility, the similarity between the temperature dependence of the traveling-wave data and previous TOF results[41] may be coincidental. Further, the nonlinear dependence on P_{SAW} means that the temperature dependence between 10 and 100 K depends on the power used. In addition, the traveling-wave experiments are performed under different conditions from the TOF experiments as the samples are continuously and strongly illuminated.

Indulging in speculation, I consider that the signal derives from two effects—the normal interaction that leads to Eq. (12), which is independent of the direction of the y axis, and an unknown interaction that reverses sign upon inversion of the y axis. A drift mobility that can be compared with the theory can be obtained by averaging the V_{AE} obtained for a $+y$ and a $-y$ faceplate thereby eliminating the anomalous term. The magnitude of V_{AE} is the same to within about 10% from one plate to the next, which is not a significant difference considering the uncertainty in P_{SAW} and h and the current noise. Thus the mobilities obtained by averaging lie at least an order of magnitude below those indicated in Figs. 15 and 16. This upper limit of the traveling-wave drift mobility is consistent with the TOF drift mobilities obtained by Kočka *et al.*,[42] and consistent with the theory of Sec. III B. Further interpretation of the data must await a better solution for the potential.

VII. CONCLUSIONS

The traveling-wave technique is a viable method to measure the drift mobility of amorphous semiconductors and provides a complement to the traditional time-of-flight technique. This paper has explored theoretical and practical aspects of the experiment—in particular, the interaction of the traveling electric field with the charge carriers in the semiconductor that creates the direct currents at each surface, the interpretation of the resulting mobility based on a model of charge transport solved for the particular boundary conditions of the experiment, and experimental methods in order to gauge systematic errors and limitations. Several of the more important results are as follows.

(1) The solutions presented here show that carrier diffusion and inhomogeneous conductivities do not produce confounding effects; data obtained from samples thinner than the diffusion length or illuminated samples or material with surface band bending can, therefore, be simply analyzed.

(2) The solution of the multiple trapping equations with the boundary conditions imposed by the experiment demonstrates that the traveling-wave drift mobility is equivalent to the TOF drift mobility when the transit time is the inverse of the traveling-wave frequency.

(3) The solution of a hopping model of low-temperature transport demonstrates that carriers with a hopping frequency equal to the traveling-wave frequency are most important for producing the direct current.

(4) Data obtained below 100 K no longer agree with the predictions of a multiple trapping model, nor do they agree with a model based on energy loss hopping. However, the anomalous dependence on SAW power and the correlation between the sign of the direct current and the direction of the $LiNbO_3$'s y axis cast doubt on the interpretation of the data as drift mobility. Future studies need to understand if the two anomalies are linked. The sign anomaly suggests that the electric potential associated with the surface acoustic wave has additional components beyond a simple traveling wave.

ACKNOWLEDGMENTS

I thank Professor Hellmut Fritzsche for suggesting this problem and for much valuable help and encouragement. I am indebted to Dr. Yoshiyuki Kaneko for the data of Fig. 19. This work was supported in part by National Science Foundation Grant No. DMR-8806197 and the Materials Research Laboratory at the University of Chicago.

[1]H. Matthews, *Surface Wave Filters* (Wiley, New York, 1977).
[2]A. Bers, J. H. Cafarella, and B. E. Burke, Appl. Phys. Lett. **22**, 399 (1973); T. Shiosaki, T. Kuroda, and A. Kawabata, *ibid.* **26**, 360 (1975); P. Das, M. E. Motamedi, and R. T. Webster, *ibid.* **27**, 120 (1975); H. Gilboa, M. E. Motamedi, and P. Das, *ibid.* **27**, 641 (1975).
[3]R. Adler, D. Janes, B. J. Hunsinger, and S. Datta, Appl. Phys. Lett. **38**, 102 (1981).
[4]K. Bløtekjaer, IEEE Trans. Electron Devices **ED-17**, 30 (1970).
[5]W. E. Spear, J. Non-Cryst. Solids **1**, 197 (1969).
[6]T. Tiedje and A. Rose, Solid State Commun. **37**, 49 (1980).
[7]J. Orenstein and M. A. Kastner, Solid State Commun. **40**, 85 (1981).
[8]T. Tiedje, in *Semiconductors and Semimetals,* edited by J. L. Pankove (Academic, Orlando, 1984), Vol. 21C.
[9]J. M. Marshall, J. Berkins, and C. Main, Philos. Mag. B **56**, 641 (1987).
[10]T. Tiedje, J. M. Cebulka, D. L. Morel, and B. Abeles, Phys. Rev. Lett. **46**, 1425 (1981).
[11]A. C. Hourd and W. E. Spear, Philos. Mag. B **51**, L13 (1985).
[12]K.-J. Chen and H. Fritzsche, J. Non-Cryst. Solids **59&60**, 441 (1983).
[13]H. Fritzsche, K.-J. Chen, and R. E. Johanson, J. Non-Cryst. Solids **66**, 199 (1984).
[14]J. Takada and H. Fritzsche, Phys. Rev. B **36**, 1710 (1987).
[15]J. Takada, Phys. Rev. B **36**, 1703 (1987).
[16]H. Ugur and H. Fritzsche, Solid State Commun. **52**, 649 (1984).
[17]H. Fritzsche, Phys. Rev. B **29**, 6672 (1984).
[18]M. Hoheisel, R. Carius, and W. Fuhs, J. Non-Cryst. Solids **63**, 313 (1984).
[19]R. E. Johanson, H. Fritzsche, and A. Vomvas, J. Non-Cryst. Solids **114**, 274 (1989).
[20]B. I. Shklovskii, H. Fritzsche, and S. D. Baranovskii, Phys. Rev. Lett. **62**, 2989 (1989).
[21]R. A. Abram and S. Edwards, J. Phys. C **5**, 1183 (1972).
[22]S. D. Baranovskii, H. Fritzsche, E. I. Levin, I. M. Ruzin, and B. I. Shklovksii, Zh. Eksp. Teor. Fiz. **96**, 1362 (1989) [Sov. Phys.—JETP **69**, 773 (1989)].
[23]D. Monroe, Phys. Rev. Lett. **54**, 146 (1985).
[24]B. A. Auld, *Acoustic Fields and Waves in Solids* (Wiley, New York, 1973).
[25]R. A. Street, J. Kakalios, and M. Hack, in *Amorphous Silicon Technology,* edited by A. Madan, M. J. Thompson, P. C. Taylor, P. G. LeComber, and Y. Hamakawa, MRS Symposia Proceedings No. 118 (Materials Research Society, Pittsburgh, 1988), p. 495.
[26]N. F. Mott, Philos. Mag. **19**, 835 (1969).
[27]S. Alijishi, J. D. Cohen, S. Jin, and L. Ley, Phys. Rev. Lett. **64**, 2811 (1990).
[28]R. E. Johanson (unpublished).
[29]G. D. Cody, in *Semiconductors and Semimetals,* edited by J. L. Pankove (Academic, Orlando, 1984), Vol. 21B.
[30]R. A. Street, J. Kakalios, C. C. Tsai, and T. M. Hayes, Phys. Rev. B **35**, 1316 (1987).
[31]J. Kakalios and R. A. Street, Phys. Rev. B **34**, 6014 (1986).
[32]This interpretation differs from that given in Ref. 14.
[33]W. B. Jackson, S. M. Kelso, C. C. Tsai, J. W. Allen, and S. J. Oh, Phys. Rev. B **31**, 5187 (1985).
[34]J. I. Pankove, *Optical Processes in Semiconductors* (Dover, New York, 1971), p. 323.
[35]H. Fritzsche, J. Non-Cryst. Solids **114**, 1 (1989).
[36]B. Yoon (private communication).
[37]R. Stachowitz, W. Fuhs, and K. Jahn, Philos, Mag. B **62**, 5 (1990).
[38]C. E. Nebel and J. Kočka, in *Amorphous Silicon Technology–1991,* edited by A. Madan, Y. Hamakawa, M. J. Thompson, P. C. Taylor, and P. G. LeComber, MRS Symposia Proceedings No. 219 (Materials Research Society, Pittsburgh, 1991), p. 563.
[39]R. E. Johanson, Yoshiyuki Kaneko, and H. Fritzsche, Philos. Mag. Lett. **63**, 57 (1991).
[40]R. S. Weis and T. K. Gaylord, Appl. Phys. A **37**, 191 (1985).
[41]C. Cloude, W. E. Spear, P. G. LeComber, and A. C. Hourd, Philos. Mag. B **54**, L113 (1986).
[42]J. Kočka, C. E. Nebel, G. H. Bauer, O. Klima, Y. Xiao, E. Šípek, and G. Juška, in *20th International Conference on the Physics of Semiconductors,* edited by E. M. Anastassakis and J. D. Joannopoulos (World Scientific, Singapore, 1990), p. 2059.

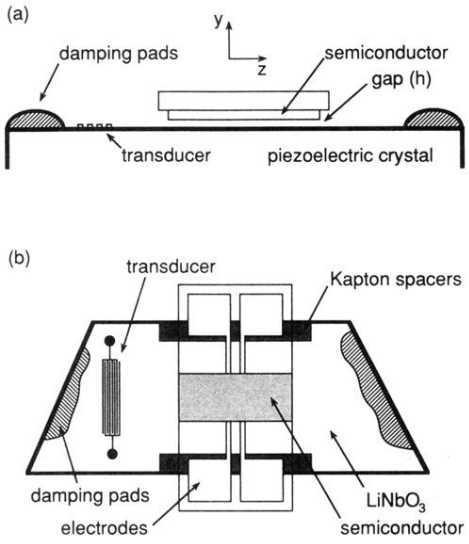

FIG. 1. A schematic diagram of the traveling-wave experiment, (a) side view, (b) top view. The $LiNbO_3$ is approximately 4 cm long and 2 cm wide.